NASA CR-134348

FINAL REPORT

COLD CATHODE GAUGE EXPERIMENT

SUPPORTED BY

NASA CONTRACT NAS 9-5964

MARCH 1974

THE UNIVERSITY OF TEXAS AT DALLAS

POST OFFICE BOX 688 RICHARDSON, TEXAS 75080

THE UNIVERSITY OF TEXAS AT DALLAS

P. O. Box 688
Richardson, Texas 75080

FINAL REPORT

FOR

COLD CATHODE GAUGE EXPERIMENT

(ALSEP)

NASA Contract NAS 9-5964

UTD Account E1473

May 14, 1966 - March 31, 1974

F. S. Johnson
Principal Investigator

D. E. Evans (JSC)
Co-Investigator

3/12/74

THE UNIVERSITY OF TEXAS AT DALLAS

COLD CATHODE GAUGE EXPERIMENT

FINAL REPORT

Contract NAS 9-5964

ABSTRACT

Cold cathode ionization gauges were left on the lunar surface as part of the ALSEP (Apollo Lunar Surface Experiment Package) on Apollo missions 12, 14, and 15. An instrument prepared for Apollo 13 did not reach the surface because of the abort of that mission. The gauges that reached the lunar surface measured the amounts of gas present in the vicinity of the ALSEP sites. The observed daytime gas concentrations were initially about two orders of magnitude greater than the nighttime observations; this was almost certainly due to contamination of the landing area by the Apollo operations and equipment, and the daytime measurements showed a decrease with time characterized by a time constant of a few months. The observed nighttime concentrations were about 2×10^{11} m^{-3}; this probably represents the true ambient level, as contaminant gases apparently freeze out at the low nighttime temperatures encountered on the moon (i.e., they are adsorbed on the lunar surface). The nighttime concentration is reasonably in agreement with the amount of neon that should be expected from the solar wind, taking into account escape from the moon and redistribution over its surface due to temperature gradients. Neon is the gas of solar

wind origin that should be most abundant; heavier gases, whose escape from the moon like neon is controlled by photoionization, are less plentiful than neon in the solar wind, and lighter gases escape more rapidly than neon due to thermal escape. Many transient gas clouds were observed, but these appear to have been released from Apollo hardware left on the lunar surface.

INTRODUCTION

Although the lunar atmosphere is known to be tenuous, its existence cannot be doubted because the solar wind striking the lunar surface constitutes an indisputable source, and there may be other sources as well. The potentially most significant source of lunar atmosphere, from the standpoint of what it could tell us, would be degassing from the lunar interior. Such degassing would provide very useful information on how planetary atmospheres originate.

The cold cathode gauge experiment (CCGE) was included in several of the Apollo lunar surface experiment packages (ALSEP) to evaluate the amount of gas present on the lunar surface. The CCGE indications can be expressed as concentrations of particles per unit volume or as pressure, which depends on the ambient temperature in addition to the concentration. The amount of gas observed was compared with the expected amount associated with the solar-wind source to obtain an indication of whether other sources of gases are present; as the

observations agreed reasonably with the expectation based on the solar wind source, no clear evidence was found of gases of other origin. Contamination from the lunar module (LM) and from the astronauts' pressure suits constituted an additional source of gas, but one that decreased with time in an identifiable way; further, it disappeared at night because of the adsorption of these gases on the lunar surface at low temperatures.

SOURCES OF LUNAR ATMOSPHERE

The one undisputable source of lunar atmosphere is the solar wind, since it is observed to impinge on the lunar surface. The evidence that the earth's atmosphere, and surely some other planetary atmospheres as well, have originated by more-or-less continuous release from the planetary interiors due to geochemical processes there leads to the possibility that this source is also a contributor to the lunar atmosphere, although the CCGE has found no clear evidence of this. Still another possible source is vaporization of meteorites following their impact on the lunar surface.

Solar Wind Source

The solar wind impinges upon the lunar surface with very little disturbance of the flow (Ness et al., 1967; Sonett & Colburn, 1967). The solar wind ions must imbed themselves in the surface materials, but

once the surface is saturated with a given constituent, that constituent must be released from the surface at the same average rate as it is brought to the lunar surface by the solar wind. After release from the surface, the neutralized particles constitute a lunar atmosphere. Those particles with sufficiently high velocities will escape from the moon just by virtue of their thermal motions, and this of course is most important for the lighter constituents.

The composition of the solar wind is reasonably approximated by cosmic abundances. The measured abundances are variable, making generalizations difficult. Bame et al. (1970) give the following relative abundances based upon solar-wind observations in spacecraft on 6 July 1969: H, 5000; He, 150; O, 1.00; Si, 0.21; and Fe, 0.17. These compare fairly well with cosmic abundances given by Cameron (1971): H, 5000; He, 410; O, 4.5; Si, 0.21; and Fe, 0.17. Helium and oxygen abundances in the solar wind on 6 July 1969 were depressed relative to hydrogen, silicon, and iron, but the relative abundances of the latter agree well with cosmic abundances. Many other measurements have been made of the He/H ratio, and an average value of 0.045 was accepted by Hundhausen (1970) based on measurements in several spacecraft programs.

Actual measurements of solar wind composition at the lunar surface by trapping in an aluminum foil give a He^4/Ne^{20} ratio of 550 (Buehler et al., 1972) and a Ne^{20}/A^{36} ratio of 36 (Geiss et al., 1971).

Measurements in lunar surface materials generally indicate less He and Ne relative to A, presumably due to the diffusive escape of these gases from the surface materials. Ilmenite samples show the least loss, and a Ne^{20}/A^{36} ratio of 33 and a He^{4}/A^{36} ratio of 7600 have been determined (Eberhardt et al., 1970), thus indicating a He^{4}/Ne^{20} ratio of 230, less than that measured in the aluminum foil. The A^{36}/Kr^{84} ratio was 2350 and the A^{36}/Xe^{132}, 16000. All ratios were given as lower limits because of the possibility of diffusive escape favoring the loss of the lighter constituent. Combining the foil and ilmenite data, the relative abundances for He^{4}, Ne^{20}, A^{36}, Kr^{84}, and Xe^{132} are 1, 1.8×10^{-3}, 5×10^{-5}, 2.15×10^{-8}, and 3.1×10^{-9} respectively. These compare with cosmic abundances (Cameron, 1971) 1, 10^{-3}, 9×10^{-5}, 1.7×10^{-8}, and 0.9×10^{-9}. Corrected for the presence of other isotopes, the relative abundances of He, Ne, A, Kr, and Xe indicated by the analyses of lunar foils and samples are 1, 2×10^{-3}, 6×10^{-5}, 3.8×10^{-8}, and 1.2×10^{-8}.

Buehler et al. (1972) report the following He^{4} fluxes ($m^{-2} sec^{-1}$) in the solar wind: 21 July 1969, 6.2×10^{10}; 19 November 1969, 8.1×10^{10}; 5 February 1971, 4.2×10^{10}; and 31 July 1971, 17.7×10^{10}. The solar wind fluxes measured in Vela satellites on these same days were 1.5×10^{12}, 1.3×10^{12}, 1.3×10^{12}, and 10^{12} (Solar Geophysical Data, Dept. of Commerce) indicating an average flux for these four days of about 40% of the average value of 3.0×10^{12} for the interval July 1965 to June 1967 (Hundhausen et al.,

1970). The He/H ratios are clearly quite variable, as can be seen from the above figures, and cannot be used to improve the average value of 0.045 quoted previously. We therefore accept 0.045 as the best value for the He/H ratio and accept the relative abundances quoted in the one previous paragraph for the noble gases. The He/H ratio of 0.045 and an average solar wind flux of 3×10^{12} m^{-2} sec^{-1} yield a helium flux somewhat greater than the average of the He determinations from the foil experiment listed above, but not as much greater as would be expected on the basis of the ratio of the average solar wind proton flux to that for the days in question.

The average thermal escape time from the moon is very short (about 10^4 sec) for light gases such as hydrogen and helium, but the escape time rises exponentially for heavier gases and is quite long (approximately 10^{10} sec or 300 years) for neon and much longer for still heavier gases. Another escape process dominates for those particles whose thermal escape is slow, and this process is ionization followed by interaction with the magnetic and electric fields of the solar wind (Manka and Michel, 1971; Manka et al., 1972). When a particle in the lunar atmosphere becomes photoionized, it immediately accelerates in response to the electric field of the solar wind. The electric field direction is perpendicular to both the solar wind velocity and the magnetic field. As the particle picks up velocity, it begins to

react to the magnetic field and finally traces out a cycloidal path whose average direction is the same as that component of the solar wind velocity perpendicular to the magnetic field. What is important with regard to loss from the lunar atmosphere is that the newly ionized particle accelerates in the direction of the solar wind electric field and its motion is not much deviated by the magnetic field until it has moved a large fraction of a gyro radius (as observed in a coordinate system moving with the solar wind). As the radii of gyration for all but the lightest ions are large compared to the moon, the heavier ions are lost, either by acceleration to space or back into the lunar surface, in a time shorter than the ion angular gyro period. As the ion gyro periods are very short compared to the times required to photoionize gas particles, it is the ionization time that controls the loss process; this time is about 10^7 sec for most particles, although 10^6 sec is a better figure for argon. The loss times may be taken to be twice the ionization times to account for the fact that about half the ions are accelerated back to the lunar surface and hence are not lost from the moon.

The distance over which the magnetic and electric fields in the solar wind are more or less uniform is very large compared to the size of the moon, approximately 0.01 AU (Jokipii, 1971).

Another loss process results from collisions between solar wind particles and atmospheric particles. For the most part, atmospheric

particles undergoing such collisions are driven back to the lunar surface and are not lost from the moon. Only around the terminator are the particles lost to space. Overall, this loss rate is small compared to that due to ionization, and it is neglected here.

Table 1 shows the expected amounts of lunar atmosphere due to the solar wind source, assuming thermal escape for hydrogen and helium and ionization loss for heavier constituents. The total amount of gas in a unit column is the product of the incident flux and the lifetime, and the gas concentration is obtained by dividing the total amount by the scale height, also shown in Table 1. Owing to the highly variable temperature over the lunar surface, the gas concentrations cannot be expected to be uniform, and the figures given in Table 1 apply to the hot portion of the lunar surface, roughly that quarter of the surface for which the solar zenith angle is less than 60°. Note that neon is expected to be the principal constituent of such an atmosphere, lighter constituents being less plentiful because their thermal escape is so rapid, and heavier constituents less plentiful because of their lower abundances in the solar wind.

The diffusion of gas over the lunar surface is a function of temperature. Gases that do not escape rapidly and that do not condense or adsorb on the cold nighttime surface distribute themselves according to a $T^{-5/2}$ concentration law, where T is the temperature of the lunar surface (Hodges and Johnson, 1968). This leads to concentrations

TABLE 1

Expected amounts of lunar atmosphere near the subsolar point due to solar wind impingement on the lunar surface.

	H	He	Ne	A	Kr	Xe
Solar wind flux atoms m^{-2} sec^{-1}	$3x10^{12}$	$1.3x10^{11}$	$2.7x10^{8}$	$8x10^{6}$	$5x10^{3}$	$1.6x10^{3}$
Escape time, sec	$3.5x10^{3}$	10^{4}	$2x10^{7}$	$2x10^{6}$	$2x10^{7}$	$2x10^{7}$
Total gas, atoms m^{-2}	10^{16}	$1.3x10^{15}$	$5.4x10^{15}$	$1.6x10^{13}$	10^{11}	$3.2x10^{10}$
Scale height, km	2000	500	100	55	25	15
Surface concentration, molecules m^{-3}	$5x10^{9}$	$3x10^{9}$	$5x10^{10}$	$3x10^{8}$	$4x10^{6}$	$2x10^{6}$
Surface pressure, torr	$1.4x10^{-13}$	$8x10^{-14}$	$1.5x10^{-12}$	$8x10^{-15}$	10^{-16}	$6x10^{-17}$

on the nightside about 26 times greater than that over the hot portion of the dayside. This effect increases the overall time constant for escape, as there is a substantial nighttime reservoir that does not participate in the escape processes. Table 2 shows concentrations of argon and neon to be expected on the day and night sides at the surface and at altitudes of 10 and 100 km, based on the solar wind source and the $T^{-5/2}$ concentration distribution law.

Internal Release of Gases

Another possible source of lunar atmosphere is gas release from internal sources. The earth and presumably other terrestrial planets have acquired their atmospheres in this fashion. Table 3 shows the average rates of release over geologic time of the principal gases arising from the earth's interior (Johnson, 1971). Table 4 shows the concentrations to be expected in the lunar atmosphere if the release rate on the moon were the same per unit mass as on earth. As in the case of Table 1, the total gas in a unit column is the product of the lifetime and the release rate, and the concentration is obtained by dividing by the scale height. The release rates per unit mass could be several orders of magnitude lower on the moon than on earth and still be important compared to the solar wind source. Release from the lunar interior is apt to be sporadic and hence gas release events might be expected to appear with considerable prominence for restricted periods of time.

TABLE 2

Expected concentrations per cubic meter of neon and argon at the lunar surface and at 10 km and 100 km above the lunar surface due to the solar wind source.

	Neon		Argon	
	Day	Night	Day	Night
Surface	4×10^{9}	11×10^{10}	1.3×10^{8}	3.5×10^{9}
10 km	4×10^{9}	7×10^{10}	1.1×10^{8}	1.6×10^{9}
100km	1.5×10^{9}	2×10^{9}	2×10^{7}	1.2×10^{6}

TABLE 3

Average rates of release over geologic time of gases from the Earth's interior.

H_2O	10^{15} molecules m^{-2} sec^{-1}
CO_2	6×10^{13}
N_2	2×10^{12}
N_e	3×10^{6}
A	2×10^{10}
Kr	2×10^{6}
Xe	1.5×10^{5}

TABLE 4

Expected amounts of lunar atmosphere near the subsolar point if the release rate per unit mass were the same as for Earth.

	H_2O	CO_2	N_2	Ne	Ar	Kr	Xe
Release rate, molecules m^{-2} sec^{-1}	1.6×10^{14}	10^{13}	3.5×10^{11}	5×10^{5}	3.5×10^{9}	3.5×10^{5}	2.5×10^{4}
Lifetime, sec	3×10^{4}	10^{7}	2×10^{7}	2×10^{7}	2×10^{6}	2×10^{7}	2×10^{7}
Total gas, molecules m^{-2}	5×10^{18}	10^{20}	7×10^{18}	10^{13}	7×10^{15}	7×10^{12}	5×10^{11}
Scale height, km	111	45	70	100	50	25	15
Surface concentration, molecules m^{-3}	5×10^{13}	2×10^{15}	10^{14}	10^{8}	1.4×10^{11}	3×10^{8}	3×10^{7}
Surface pressure, torr	1.3×10^{-9}	5×10^{-8}	3×10^{-9}	3×10^{-15}	4×10^{-12}	8×10^{-15}	10^{-15}

Meteorite Impact and Vaporization

Meteorite impact on the lunar surface will release gas by vaporization. The rate of impact is near 10^{-6} impacts m^{-2} sec^{-1} for meteorites of mass 2×10^{-12} kg and smaller, giving a rate of mass inflow of 2×10^{-18} kg m^{-2} sec^{-1}; larger meteorites make only a small contribution by comparison. Although the entire mass of the meteorites may be volatilized upon impact, only a small fraction of this mass will be in the form of vapors that may persist in gaseous form, as opposed to condensing on the lunar surface. Thus meteorite vaporization upon impact can amount to only a very small source of atmospheric gas compared to the solar wind - about 3×10^{7} ϵ molecules m^{-2} sec^{-1}, or 10^{-5} ϵ lower than the solar wind source, where ϵ is the fraction of meteorite weight that appears in the form of gas after impact.

THE COLD CATHODE GAUGE

The vacuum gauge that was included in the Apollo Lunar Surface Experiment Package is a cold cathode ionization gauge built by Norton Research Corporation. The general configuration is shown in Figure 1. The envelope and electrodes are of stainless steel. An axial magnetic field of about 0.090 tesla is provided by a permanent magnet. The orifice was closed but not sealed with a spring loaded cover that was released by an electrical impulse to a squib motor. A photograph of

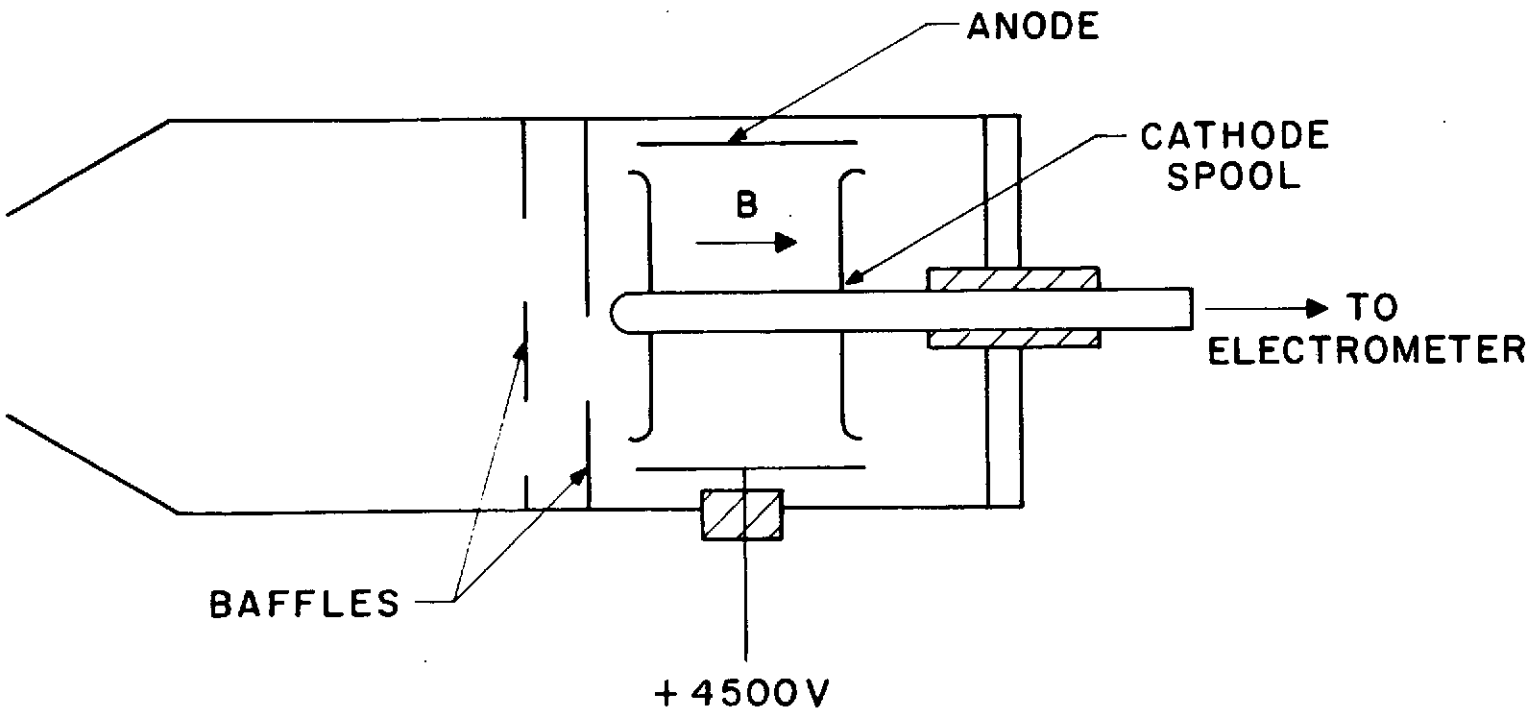

Figure 1 Schematic representation of the cold cathode ionization gauge.

the gauge and its magnet is shown in Figure 2. To reduce the possible effects of the magnet on other instruments, a magnetic shield can was mounted around the gauge and its magnet. The electronics for the Cold Cathode Ionization Gauge were contained in the Suprathermal Ion Detector Experiment (SIDE), and the command and data handling systems of the SIDE served the gauge. The gauge itself was separable from the SIDE package and connected to it by a cable about a meter long.

The response of the gauge in terms of cathode current versus pressure is shown in Figure 3. The gauge of course is really sensitive to gas density rather than pressure, and the response curve shown in Figure 3 is for room temperature. A temperature sensor was attached to the gauge envelope so as to permit corrections to be made to the gauge response based on the wide variations in temperature encountered on the lunar surface, about 100 to 400 K. The gauge response is also somewhat dependent upon gas composition, and the calibration was for nitrogen. As the composition of lunar atmospheric gases is not known, a fundamental uncertainty is introduced into the interpretation of the data, and the results are presented as if the gas were nitrogen. The difference between the nitrogen equivalent pressure and the true pressure is probably less than a factor of two.

The gauge anode is connected to a +4500 $\pm$ 200-volt power supply, which is shown diagrammatically in Figure 4. The supply consists basically of a regulator, converter, voltage-multiplier network,

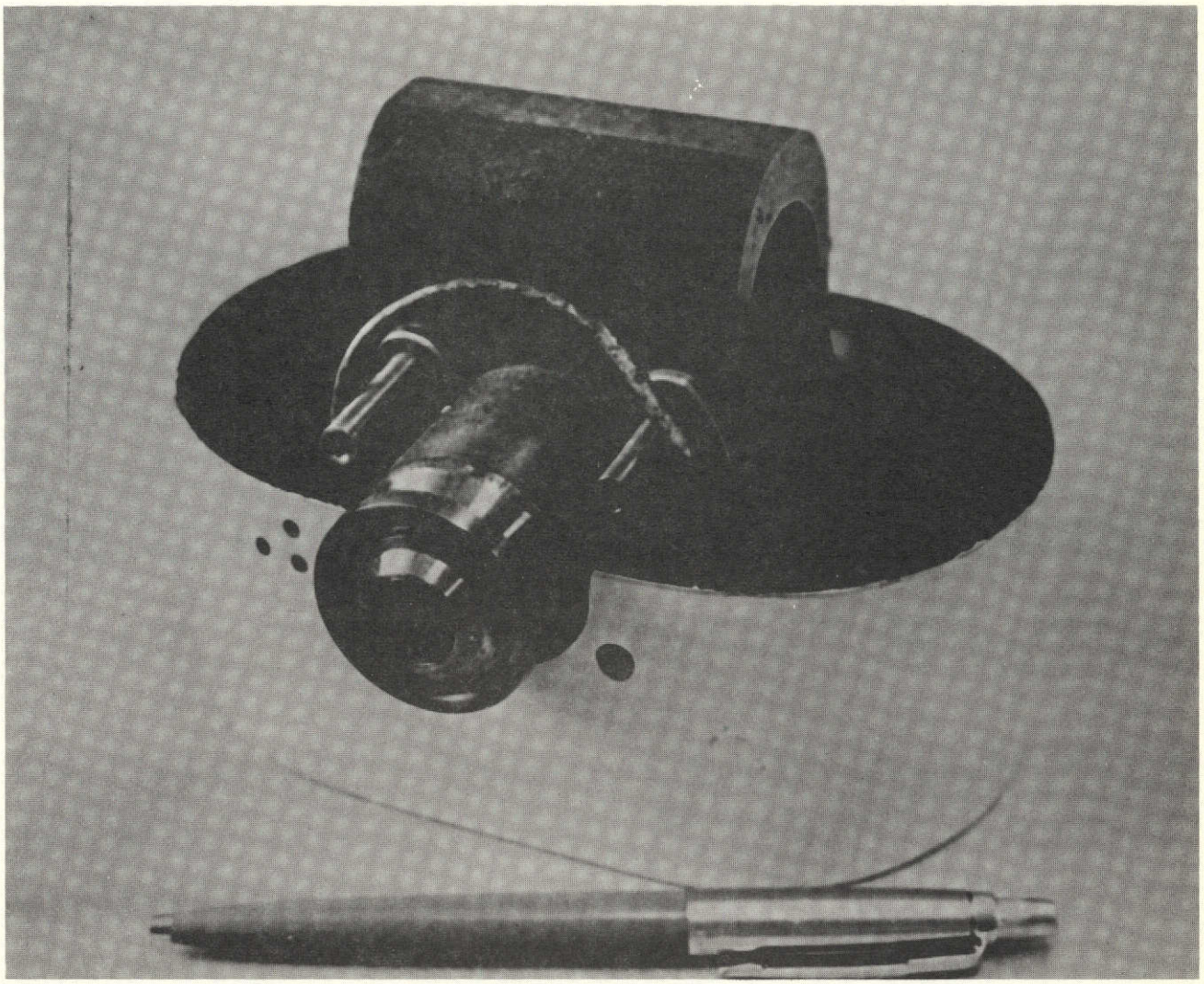

Figure 2 The cold cathode ionization gauge flown in the Apollo missions. Half of the magnetic shield can has been removed.

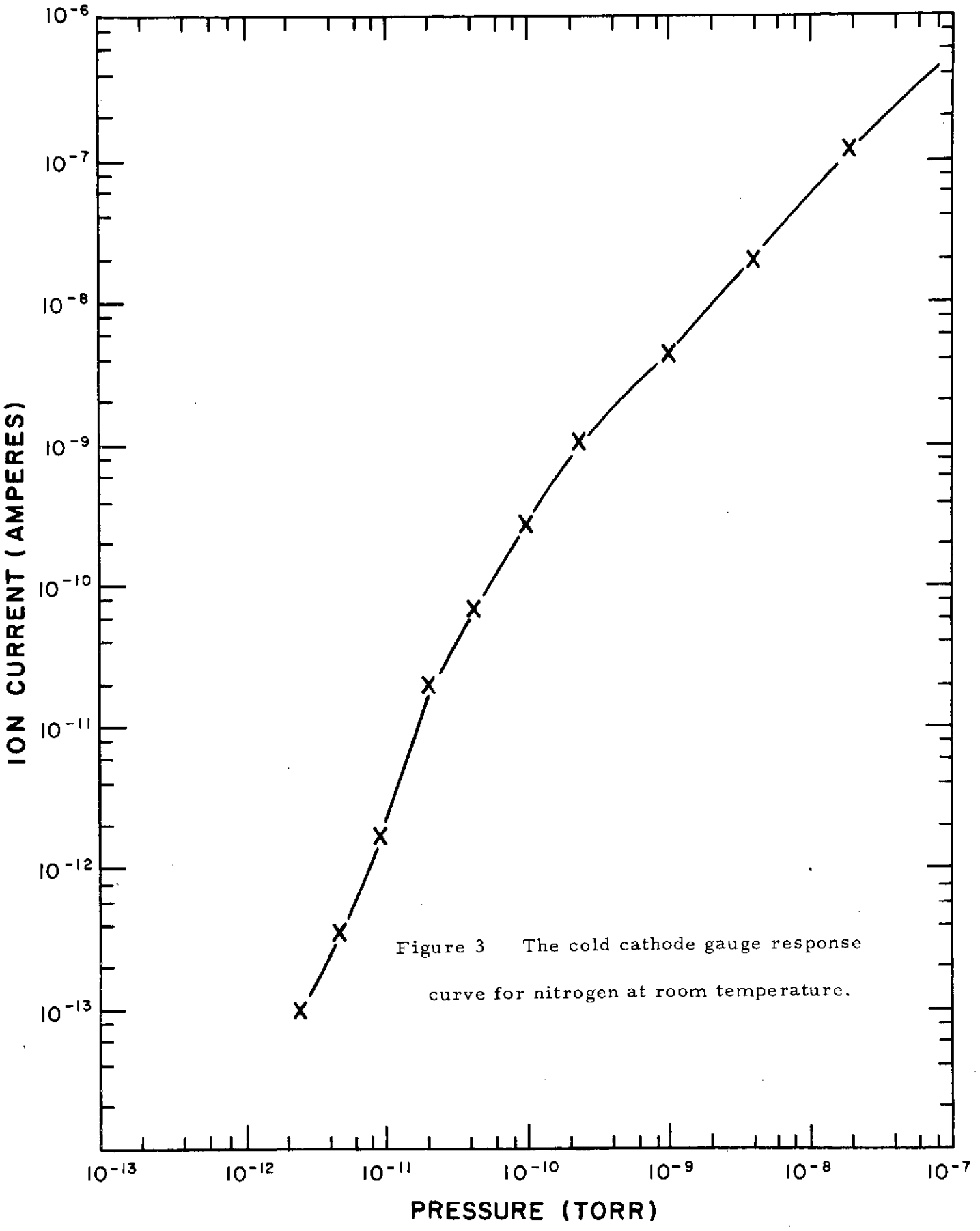

Figure 3 The cold cathode gauge response curve for nitrogen at room temperature.

71-7

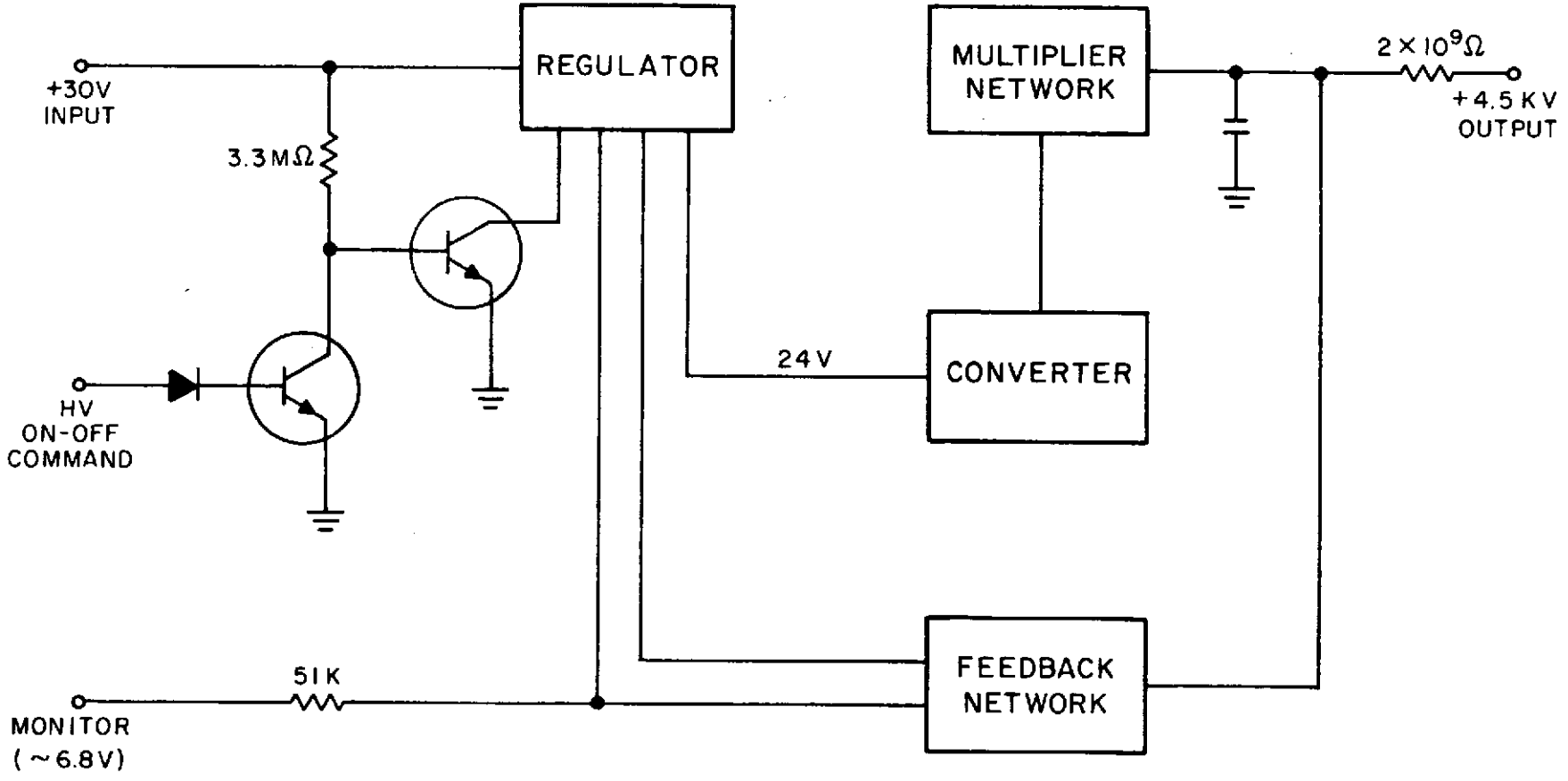

Figure 4 The high voltage power supply. 71-8

and a feedback network to the low-voltage supply. The regulator furnishes 24-volt output for conversion to a 5-kHz squarewave that is applied to the converter transformer. The output of the transformer goes to a voltage-multiplier network consisting of stacked standard doublers. The output is filtered and applied to the gauge anode and also divided down in order to provide a monitor signal. A high resistance in the connection to the gauge anode provides overload protection for the gauge and power supply, limiting the maximum current to about 2 microamperes. The output regulation is within 2% for load currents up to 1 microampere.

The gauge cathode is connected to an auto-ranging, auto-zeroing electrometer that measures currents in the range 10^{-13} to 10^{-6} ampere with an output of -15 millivolts to -15 volts. The output goes to an analog-to-digital converter for transmission over the ALSEP data link to earth. The electrometer consists of a high-gain, low-leakage, differential amplifier with switched high-impedance feed-back resistors for range changes. The output voltage and input current are related by

$$E = R_f(I_i + I_l)$$

where E is the electrometer output, I_i the input current, I_l the leakage current, and R_f the feedback resistance. When the input current is zero, the output voltage does not go to zero because of leakage and

other factors, and the output voltage can be expressed as $R_f I_1$; this voltage is the zero offset voltage, and it is cancelled by introducing a compensating error voltage from the auto-zeroing network into a second grid in the electrometer tube, as indicated in Figure 5. Auto zeroing is accomplished by disconnecting the sensor by opening relay S1 and switching in the auto-zeroing amplifier in a feedback network to the second grid by closing S3 for a short interval; capacitor C1 holds the zero-correcting potential until the next auto-zeroing cycle. Relay S2 connects the sensor to ground during the interval that it is disconnected from the electrometer.

The electrometer operates in three automatically selected overlapping ranges: (1) 10^{-13} to 9×10^{-11} amp, (2) 3.3×10^{-12} to 3.2×10^{-9} amp, and (3) 10^{-9} to 9.3×10^{-7} amp. The electrometer has strong feedback to maintain the input grid potential at nearly zero. Automatic range switching is accomplished by the switching of two feedback resistors R_1 and R_2 across permanent feedback resistor R_3, as indicated in Figure 5. To control the range changes, the electrometer output is compared against -15 mV and -15 V references by means of comparators. The output of these comparators pass to a logic circuit that drives relays S4 and S5 and generates a range signal for transmission to earth; a signal is also generated to select the proper current generators for calibration by closing S6, S7, or S8 and S9, S10, or S11.

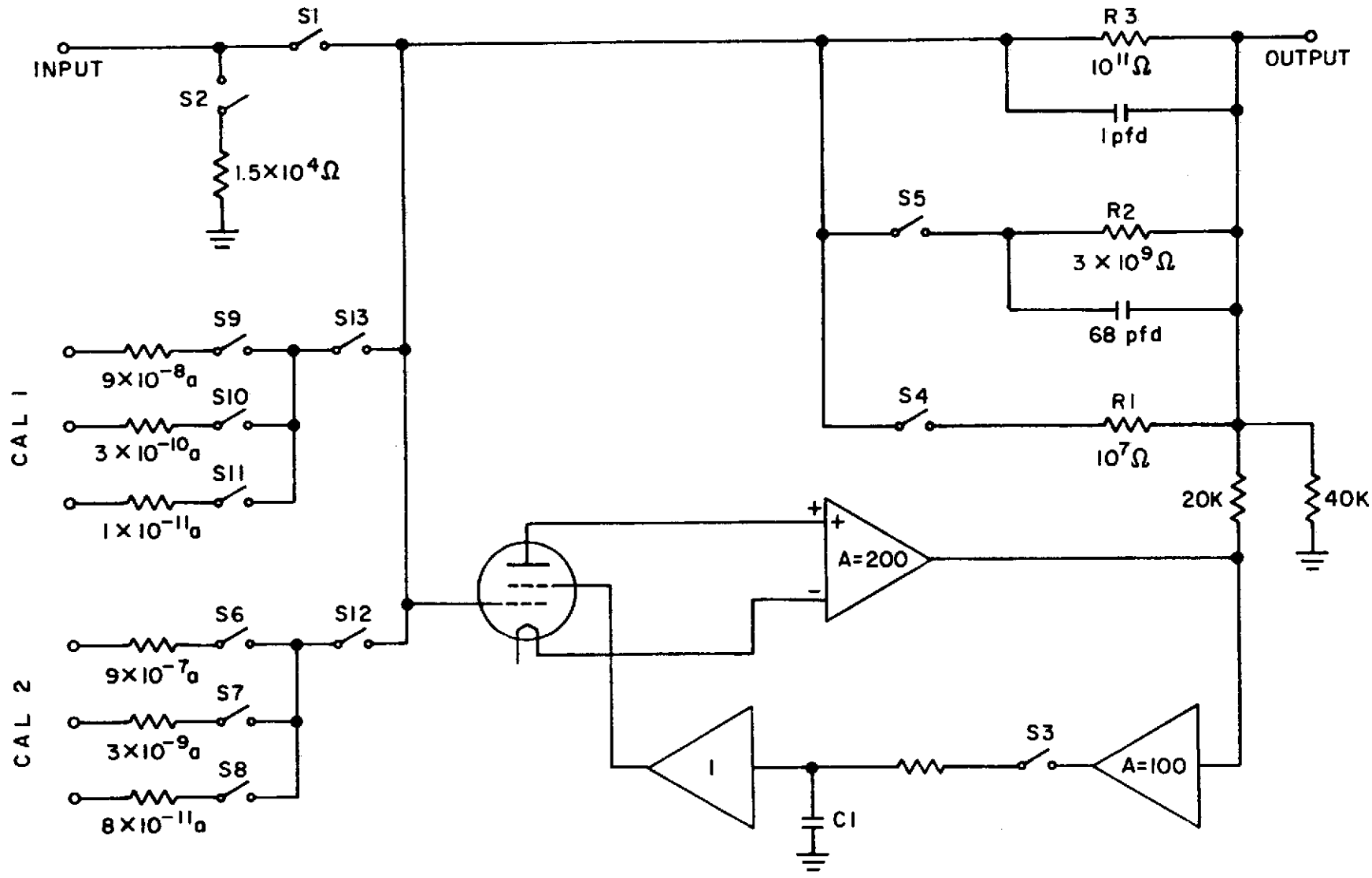

Figure 5 The electrometer and auto-zeroing circuit with calibration

The normal operating sequence of the electrometer circuit requires approximately 2 1/2 minutes per cycle, including a 16-second calibrate function and auto-zeroing. The first operation is the zero check and correction; S1 is opened and S2 is closed to disconnect the gauge and then after about 9 seconds the output of the electrometer is sampled, followed by a closing of S3 for about 2 seconds to accomplish the autozeroing. This is followed by the first step of the calibration cycle, accomplished by closing S13, and then by the second step, accomplished by opening S13 and closing S12. Following the calibrate cycle, the gauge is reconnected to the electrometer. The electrometer output is then sampled five times at 2.4 second intervals and 3 times at 38 second intervals.

Several other modes of operation were available upon ground command, although these were not much used in normal operation of the gauge. The normal mode of operation involved the complete sequence of 128 frames of data from the SIDE instrument. The other modes were:

(1) Reset at 79, which involved shortening the SIDE sequence to 79 frames. This sequence involved 5 readings of the gauge at 2.4 second intervals, followed by another reading 38 seconds later and then a 35 second delay before the repeat of the sequence. There was no calibrate cycle and no autozeroing in this mode.

(2) Reset at 39, which involved shortening the SIDE sequence to 39 frames. This sequence involved 5 readings at 2.4 second intervals

followed by a 35 second delay before the repeat of the sequence. There was no calibrate cycle and no autozeroing in this mode.

(3) Reset at 10, which involved shortening the SIDE sequence to 10 frames. This sequence involved repeated readings at 2.4 second intervals with no calibration or autozeroing.

(4) Forced calibration. This sequence involved calibration cycles only, repeated at 12 second intervals.

GAUGE CALIBRATION

A calibration curve was supplied for each gauge by the manufacturer, Norton Research Corporation (NRC), showing the gauge response to nitrogen at room temperature. The calibration was made on a small ultra high vacuum system using a Modulated Bayard-Alpert Gauge (MBAG) as the reference.

In addition to the calibration at NRC, two gauges were independently calibrated by Midwest Research Institute (MRI) in Kansas City and one gauge was calibrated at Langley Research Center by Langley and University of Texas at Dallas personnel.

Calibration at Norton Research Corporation

The vacuum system employed for calibration at NRC is a small, all-metal, ion-pumped system capable of achieving true pressures of about 1×10^{-11} torr nitrogen equivalent. The basic ultra

high vacuum pump is a small 8 liter sec^{-1} Ultek ion pump. The system was intentionally designed with a low speed pump to reduce pressure differences and to note the true outgassing rates of the gauges under study. Large ion pumps tend to make the gauges look much more gas-free than they really are.

Calibration was accomplished by comparison with an Electron Technology Inc. Modulated Bayard-Alpert Gauge (MBAG). The modulated gauge was calibrated in the range from 10^{-6} torr to 10^{-10} torr using an NRC Multiple Orifice Calibration system built for the Heath Calibration Center (Air Force), Ohio. The calibration data are on file at NRC. In using the MBAG as a secondary standard, it is recognized that uncertainties (especially in the so-called x-ray limit caused by electron impact on the grid) are inevitable, even in the MBAG. Therefore, other techniques were relied on to establish the true x-ray limit. After the true x-ray limit was established by observing how the collector current varied with grid-voltage when the emission current was held constant, the observed or anomalous x-ray current was compared to it. The modulation technique yielded the anomalous current.

In order to successfully use the modulation technique at pressures below 1×10^{-10} torr, precise readings of the ion currents I_1 and I_2 are necessary. (I_1 is the ion current with the modulator at grid potential, and I_2 the current with the modulator at ground potential.) To achieve the necessary precision, the ion current from the MBAG was read from the voltage output of a Keithley 610 BR Electrometer by a

digital voltmeter. The two modulation currents, I_1 and I_2 were read to three significant figures.

The MBAG emission current meter, located in an NRC 753 ion gauge controller, was calibrated against a Weston Standard (Model 931) milliammeter.

The CCIG current was read from another Keithley 610BR Electrometer, using the panel meter. The anode potential for the gauge was derived from a regulated high-voltage supply and was measured by a Keithley high-voltage probe.

Gas was admitted through a purged line into a lower manifold section of the system. This gas then leaked through the ultra-high-vacuum valve and up to the main manifold. Care was taken to insure that stable pressure was obtained in all gauges before readings were taken.

Calibration at Midwest Research Institute

Two gauges were calibrated at Midwest Research Institute (MRI). The first was serial number 12 (S/N 12) from Flight Unit No. 1 spare, on which calibration runs were made from 17 August to 9 September 1967, and the second was S/N 2 from Flight Unit No. 1, on which calibration runs were made on 28 April and 9 May 1968.

The results of the calibration of S/N 12 are shown in Figure 6; this figure is taken from the MRI report of 4 October 1967, but the

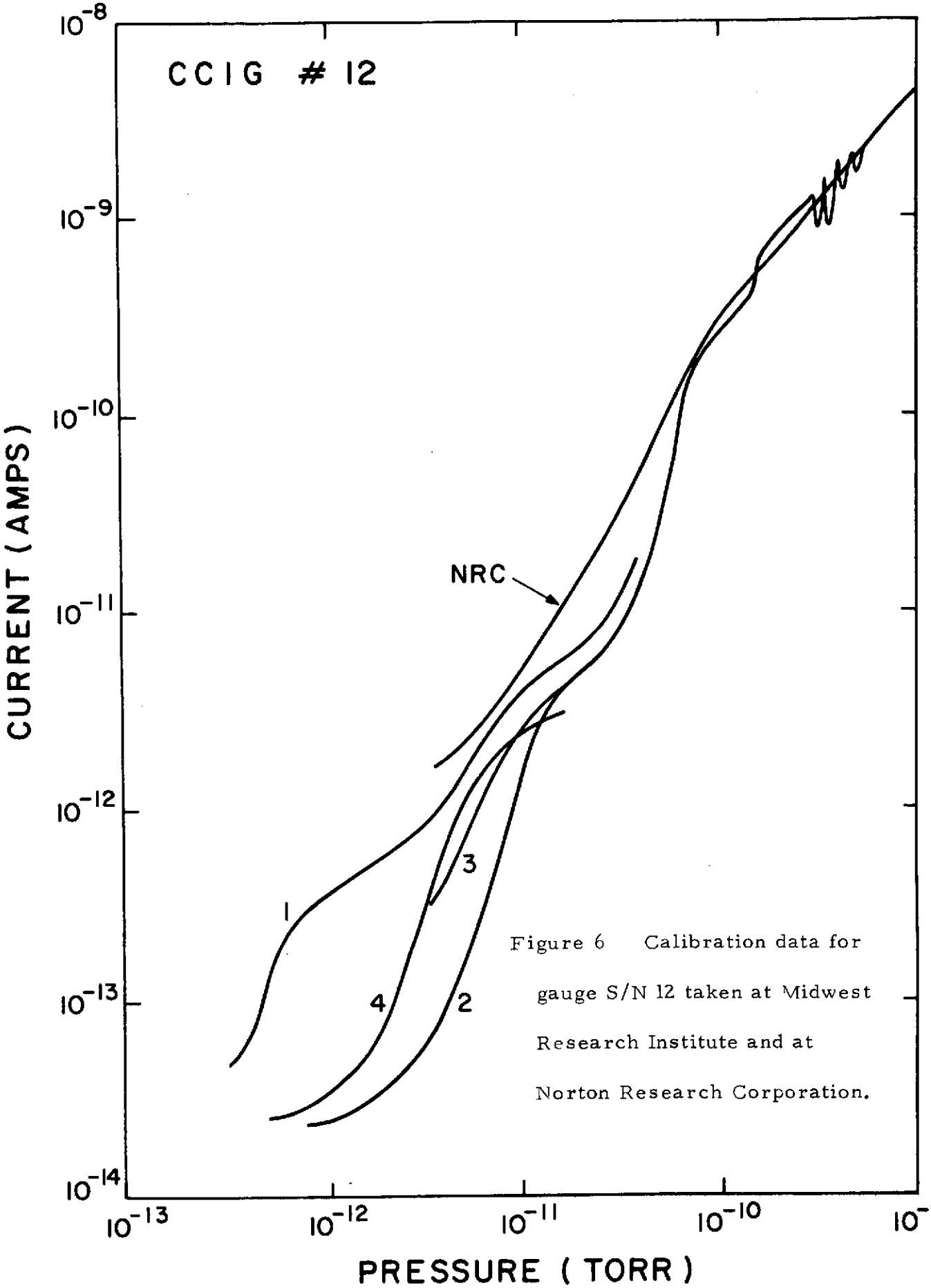

Figure 6 Calibration data for gauge S/N 12 taken at Midwest Research Institute and at Norton Research Corporation.

calibration supplied by NRC with the gauge has been added. Three points should be noted:

(1) The MRI results indicate a dip in sensitivity not indicated by NRC in the region 10^{-10} to 10^{-11} torr.

(2) Only the first calibration run (on 17 August) lies near the extrapolation of the NRC calibration. After this run, the gauge showed consistently lower sensitivity at pressures below 10^{-11} torr. This has been attributed to a decrease in magnet strength, possibly associated with thermal shock as a result of emersion in liquid nitrogen, which occurs during the calibration run.

(3) Excluding the 17 August data, the sensitivity of the gauge appears to be constant within better than a factor of two from the mean, but more than a factor of ten lower in sensitivity at pressures near 10^{-12} torr than would be estimated by extrapolation of the NRC calibration curve.

The results of the calibration of S/N 2 are shown in Figure 7 again with the NRC calibration shown for comparison. Three points should be noted here:

(1) The sensitivity is not uniform. The differences between the calibrations of 9 May and 26 April suggest that the precision of cold cathode gauges is no better than a factor of two at pressures below about 10^{-10} torr.

(2) The sensitivity of this gauge as measured by MRI is significantly lower than that determined by NRC at all pressures. The difference is small at pressures above 10^{-10} torr, but almost a factor of ten at

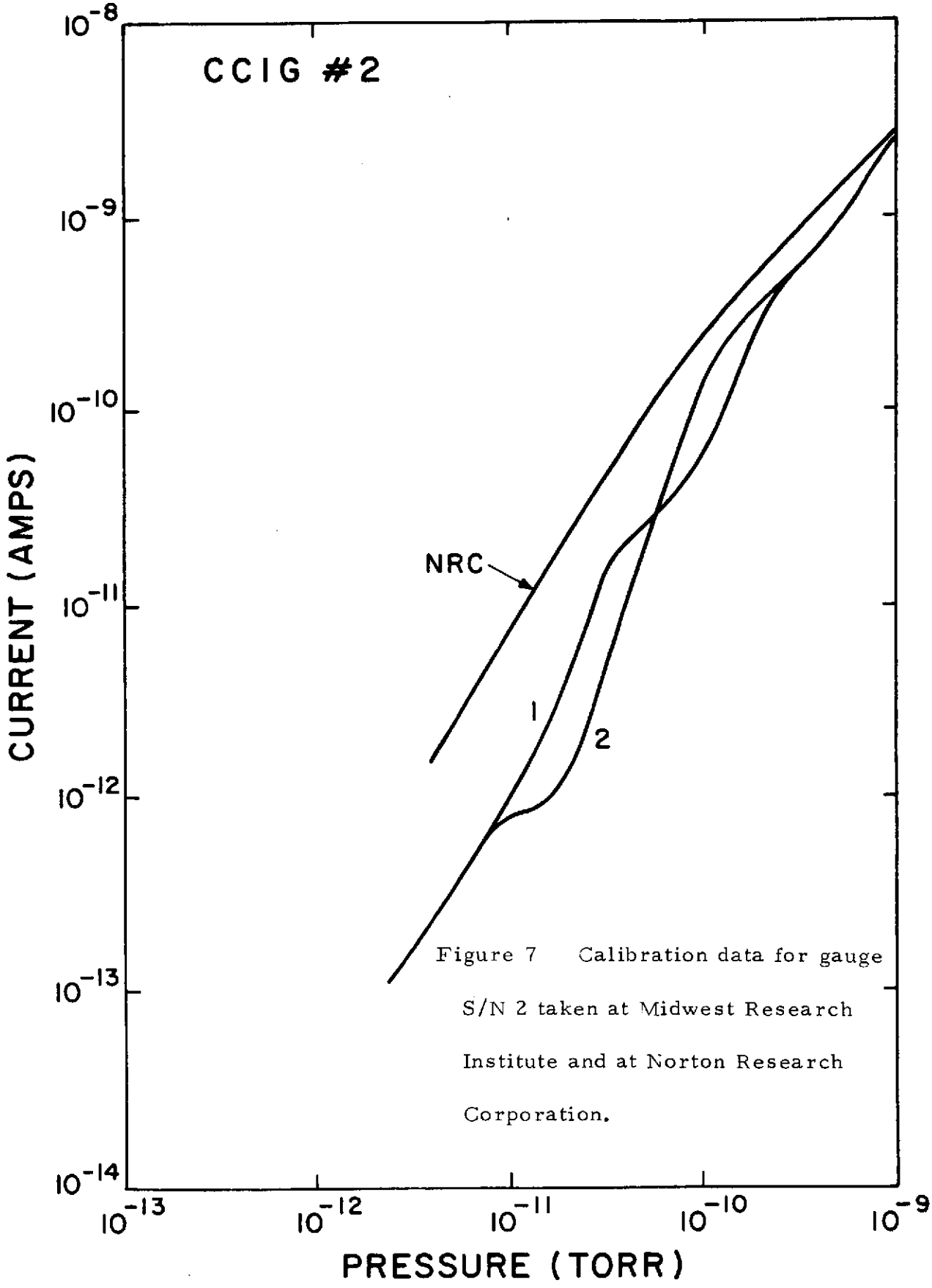

Figure 7 Calibration data for gauge S/N 2 taken at Midwest Research Institute and at Norton Research Corporation.

71-17

pressures below 10^{-11} torr. Some of this difference may be due to a reduction in magnet strength between the two calibrations. After the return of this gauge to NRC, the magnet strength was found to be .0835 tesla as compared to .092 tesla when the gauge was originally assembled. If the difference between the NRC and MRI calibrations is due to the change in magnetic field strength, then of course the MRI calibration is the appropriate one to use after the gauge has aged a while. If this is not the explanation, then the difference must be attributed to other factors, such as characteristics of the calibration procedure or a difference in standards at the two laboratories.

(3) In the initial response run, the gauge did not come into operation until the pressure was elevated to 5×10^{-11} torr. Cold cathode gauges are often slow to start at very low pressures, and this was apparently a manifestation of this property. This was not a problem in the ALSEP application because there was a substantial background pressure (due to adsorbed rocket exhaust) around the gauge when it was first turned on.

In summary, the calibration runs disclose the main limitations that are known to exist with cold cathode gauges. They tend to oscillate in some pressure regions, they are slow to start at very low pressures, they have discharge-mode changes which change the output by a factor of two or greater, and their accuracy is limited to about a factor of two below 10^{-10} torr. Examples of these characteristics are shown

later in this report in the subsection on Anomalies in the section on Operational History. Further, these calibration runs show the lack of agreement that exists between different calibration devices and techniques, and they drew attention in this case to the dependence of gauge sensitivity on magnetic field below 10^{-10} torr.

Magnetic Field Strength

The lack of agreement between the MRI and NRC calibration led to a examination of factors that might cause, or contribute to, the difference. The most important result of this inquiry was the discovery that the magnet strength on gauge S/N 12 had decreased from 0.0897 tesla when it was originally calibrated at NRC, to 0.0780 tesla when it was returned to NRC after the MRI calibration, and that the gauge sensitivity at low pressure was dependent upon field strength. The specified field strength was 0.090 ± 0.005 tesla. Figure 8 shows the sensitivity of gauge S/N 12, as measured at NRC, for three field strengths, 0.0935, 0.0897, and 0.0780 tesla.

The magnets on gauge S/N 2 also decreased in strength between the time of its initial assembly and its return to NRC after calibration at MRI. In this case, the reduction was not as great, the change being from 0.0920 to 0.0831 tesla.

The cause of the decrease in magnetic field strength was not determined. Tests were run in which the magnets were subjected to various kinds of abuse, and decreases in field strength were noted, but

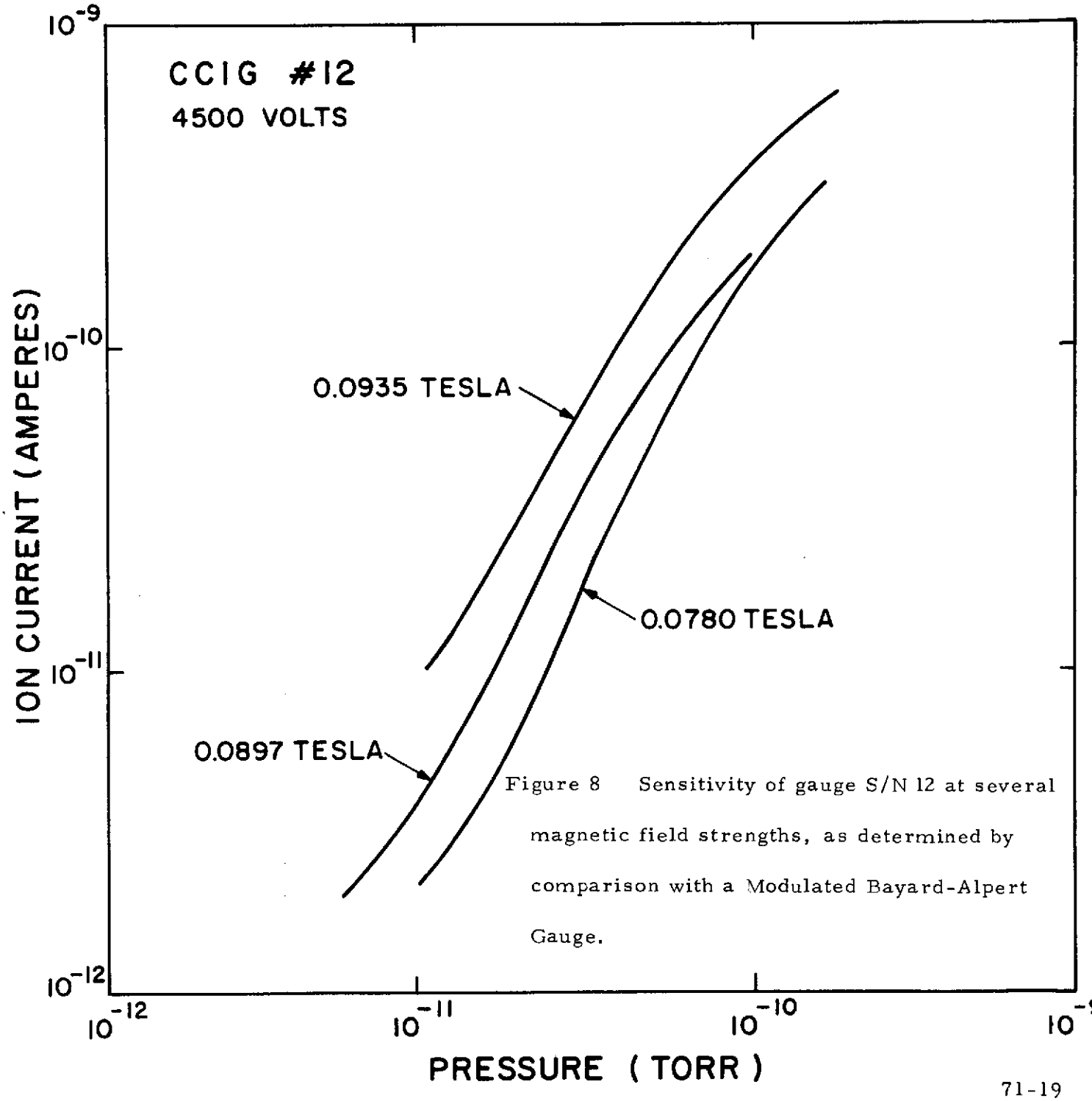

Figure 8 Sensitivity of gauge S/N 12 at several magnetic field strengths, as determined by comparison with a Modulated Bayard-Alpert Gauge.

71-19

none were as great as the decrease that occurred with the magnet on gauge S/N 12. The tests included normal handling, thermal shocks by emersion in liquid nitrogen, mechanical shock, etc., and the maximum field reduction that resulted was about 5% or 0.005 tesla. After recognition of this problem, a program of monitoring magnetic field strength on all gauges was undertaken in order to detect any tendency of the magnets to age and change in field strength. These measurements disclosed a tendency for magnets to decrease by 0.005 to 0.010 tesla before stabilizing.

Discussion

The MRI calibrations showed consistently lesser sensitivity below 10^{-10} torr than did the NRC. Part of this difference is undoubtably due to the decrease in magnet strength between the two calibrations. However, the differences are probably greater than can be explained on this basis alone. Other factors that may have been involved include the temperature differences during calibration, and the calibrating gas. The gauges were cooled to liquid nitrogen temperature during the MRI calibrations, but not during those at NRC. In general, gauge response to gas density is not a function of temperature, but some small difference may be attributed to this. The MRI calibrations were performed with helium, while both helium and nitrogen were used at NRC. The gauge sensitivity is less for helium than for nitrogen, but

it is assumed that a simple factor can be used to correct for this, and that the gauge performances for helium and nitrogen are the same when the currents are the same - a point that has been well established in general at higher pressures. Especially at pressures below 10^{-10} torr, it is possible that some of the differences are associated with the different gases used in calibration.

Overall, it was concluded that the MRI calibrations are the more appropriate, as they are representative of aged magnets. Further, use of helium as a calibrating gas is probably preferable in light of the fact that another noble gas, neon, is probably the principal constituent of the lunar atmosphere. Any noble gas is apt to produce a response curve that is more typical of other noble gases than of non-noble gases. In any case, the differences in calibration are small above 10^{-10} torr, whereas errors are apt to be of the order of a factor of two from 10^{-10} to 10^{-11} torr, and considerably larger, even a factor of ten, from 10^{-11} to 10^{-12} torr. However, this is the present state-of-the-art for vacuum gauge calibration in this pressure range.

GAUGE CALIBRATION AT LANGLEY RESEARCH CENTER

Gauge serial number 13 was calibrated at Langley Research Center on April 27, 1972 by Langley and University of Texas at Dallas personnel. The calibration was performed using the Langley Molecular Beam Pressure Technique (Smith, 1969).

A molecular beam is formed by a stream of molecules effusing from a small aperture source into an evacuated chamber, where its direction is defined by collimating apertures. A high pressure gas source is used to maintain inlet pressures from 0.1 to 10^4 torr, at a constant known temperature between 295 K and 301 K. This known pressure is dropped from 4 to 7 orders of magnitude through a selected porous plug in the manner described by Owens (1965) into a molecular furnace. From there the gas effuses through an aperture in the furnace as a cosine distribution. All but the core of this effused gas is stripped off by liquid helium cooled baffles and the remaining core of gas forms the molecular beam.

In order to know the beam fluxes precisely, the source pressure must be accurately measured. This is done using a rotating piston gauge as a high pressure measurement standard. The high source pressure is then reduced by a known factor as the gas is passed into a molecular furnace. In this application a porous silicate glass plug was used to provide the pressure attenuation.

The conductance (C_p) of the plug was experimentally determined (in situ) for all test gases. For a known volume of gas on one side of the porous plug in a steady-state flow condition, molecular conservation requires that

$$P(t) = P_o \, \epsilon^{-C_p t/V}$$

where the initial source pressure is P_o, and the volume is V. If pressure P(t) and time t are recorded, the conductance can be determined from experimental data over a given pressure range.

In order to make accurate beam flux calculations using molecular theory, it is required that the gas initially be in equilibrium at some known temperature. A molecular furnace is used for this purpose, where the wall temperature is maintained at the same constant value as the gas source. The temperatures of the molecular furnace and the gas source were monitored and recorded. Temperature variations were less than $\pm$ 0.2 K. Therefore, errors associated with molecular furnace and source temperature (298 K) were negligible. Gas molecules are assumed to equilibrate rapidly to the wall temperature of the molecular furnace.

The molecular furnace has a precision aperture from which a collisionless beam emerges with an angular distribution according to the Knudsen cosine law. Calculations from molecular theory (Smith, 1969) show that the beam equivalent flux density is given as:

$$\Gamma_b = \frac{1}{2}\left(\frac{r_a}{\lambda}\right)^2 \frac{C_p}{C_a}\left(\frac{2}{\pi m k T_f}\right)^{1/2} P_s \text{ molecules } m^{-2} \text{ sec}^{-1}$$

where

C_a = conductance of furnace aperture, 3.4 liters sec^{-1} for argon, 4.05 liters sec^{-1} for nitrogen, and 4.8 liters sec^{-1} for neon at 298 K

C_p = conductance of porous plug, 3.33×10^{-6} liters sec^{-1} for argon, 4.38×10^{-6} liters sec^{-1} for nitrogen and 4.38×10^{-6} liters sec^{-1} for neon at 298 K

k = Boltzman's constant, 1.38×10^{-23} joule deg^{-1}

λ = distance from beam aperture to plenum inlet, 2.07 m

m = mass per molecule

P_s = source pressure, newtons m^{-2}

r_a = furnace aperture radius, 0.0033 m

T_f = furnace temperature, 298 K

Γ_b = number of molecules per second impinging on each square meter of the inlet (plenum) opening

Three runs were made using nitrogen, argon, and neon. The results of these runs are shown in Figure 9.

The original NRC calibration and the Langley nitrogen calibrations are shown in Figure 10, along with the calibration curve used for both flight gauges. The calibration at Langley indicated that the gauge was a little less sensitive than indicated by the NRC calibration. This agrees with the results at Midwest Research.

The calibration curves used for the flight gauges were developed prior to the calibration at Langley. This was done taking the NRC curve and decreasing the sensitivity in the lower density regions. The amount of change in magnet strength was a factor in the development. The curves developed had a sensitivity between the NRC and MRI curves.

Figure 9 Calibration data for gauge S/N 13 taken at Langley Research Center for nitrogen, argon, and neon.

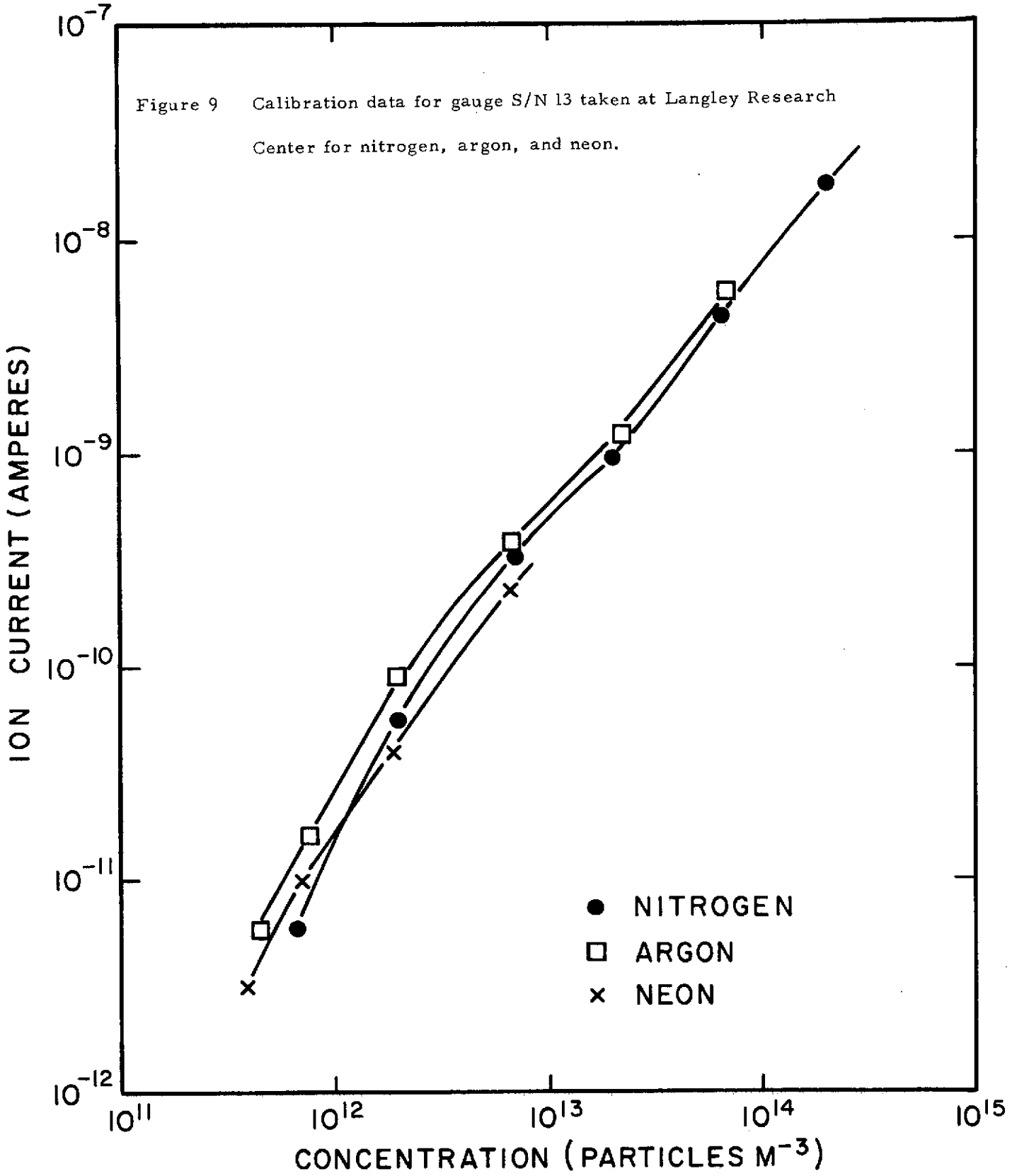

Figure 10 Calibration data for gauge S/N 13 taken at Langley Research Center and at Norton Research Corporation, along with the sensitivity curve adopted for the flight gauges.

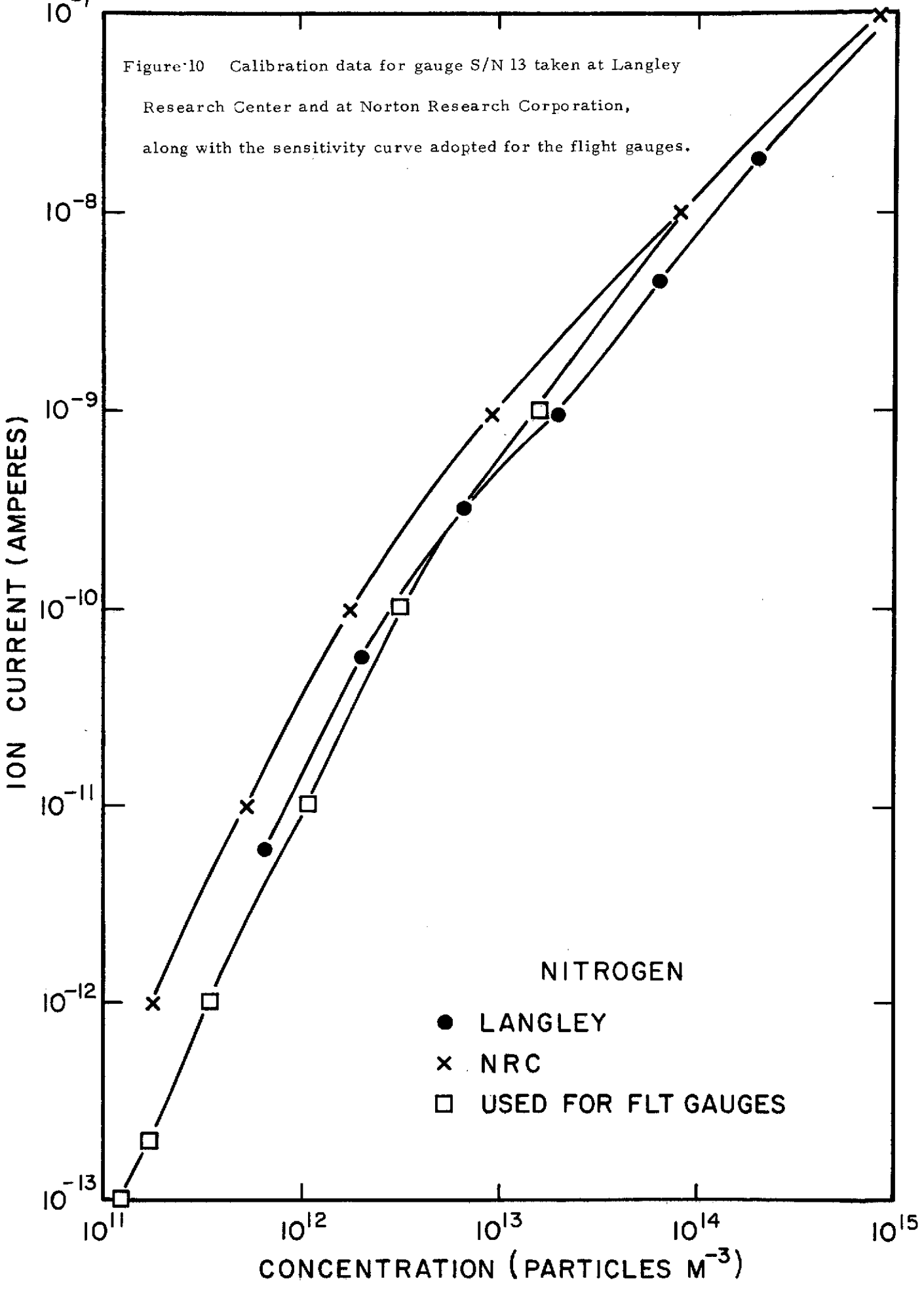

The fact that the later calibration at Langley produced a curve very close to the corrected curve for that particular gauge (as shown in Figure 10) substantiated the development technique used to obtain the calibration curves for the flight gauges.

Results obtained by the Lunar Mass Spectrometer (Hodges et al., 1973) regarding total density at nighttime tend to verify the calibrations curve used for the Cold Cathode Gauge.

DEPLOYMENT

Apollo 12

On deployment of the Suprathermal Ion Detector Experiment (SIDE) the Cold Cathode Gauge was removed from its storage position in the SIDE. It was intended that the gauge opening look out horizontally and poleward, generally away from the descent stage. The cable proved to be cold and stiff, and in the lunar gravity, even the relatively heavy gauge and magnet was not adequate to hold the cable out straight. Consequently, the gauge tipped so as to face in a generally upward direction, despite repeated efforts by Astronaut Conrad to properly deploy the gauge. As a result of the deployment problem, the cable for subsequent experiments was redesigned to eliminate some of the stiffness.

Apollo 14

The Apollo 14 CCGE is shown in the left foreground of Figure 11 as it is deployed on the lunar surface. The dust cover over the entrance aperture was removed by an electrical command from earth through the central station after the deployment of all the experiments was complete. A one-meter cable, which also can be seen in the picture, connected the gauge to its electronics in the large upright white package which also contained the Suprathermal Ion Detector Experiment (SIDE). Stiffness of the cable again made deployment difficult, but a proper orientation of the gauge was achieved. The gauge and electronics were placed approximately 20 meters from the remaining experiments, the central station, and the radioisotope thermo-electric generator, all of which are visible in the background. This lunar surface deployment configuration provided a clear field of view for the gauge since it did not "look" directly at any of the other surface instruments or at the manned lunar landing module.

Apollo 15

The Apollo 15 CCGE is shown deployed on the lunar surface in Figure 12. This gauge was attached to the lower end of the extended leg of the SIDE to provide easier deployment of both the gauge and the SIDE experiment. The extended leg also served an additional purpose

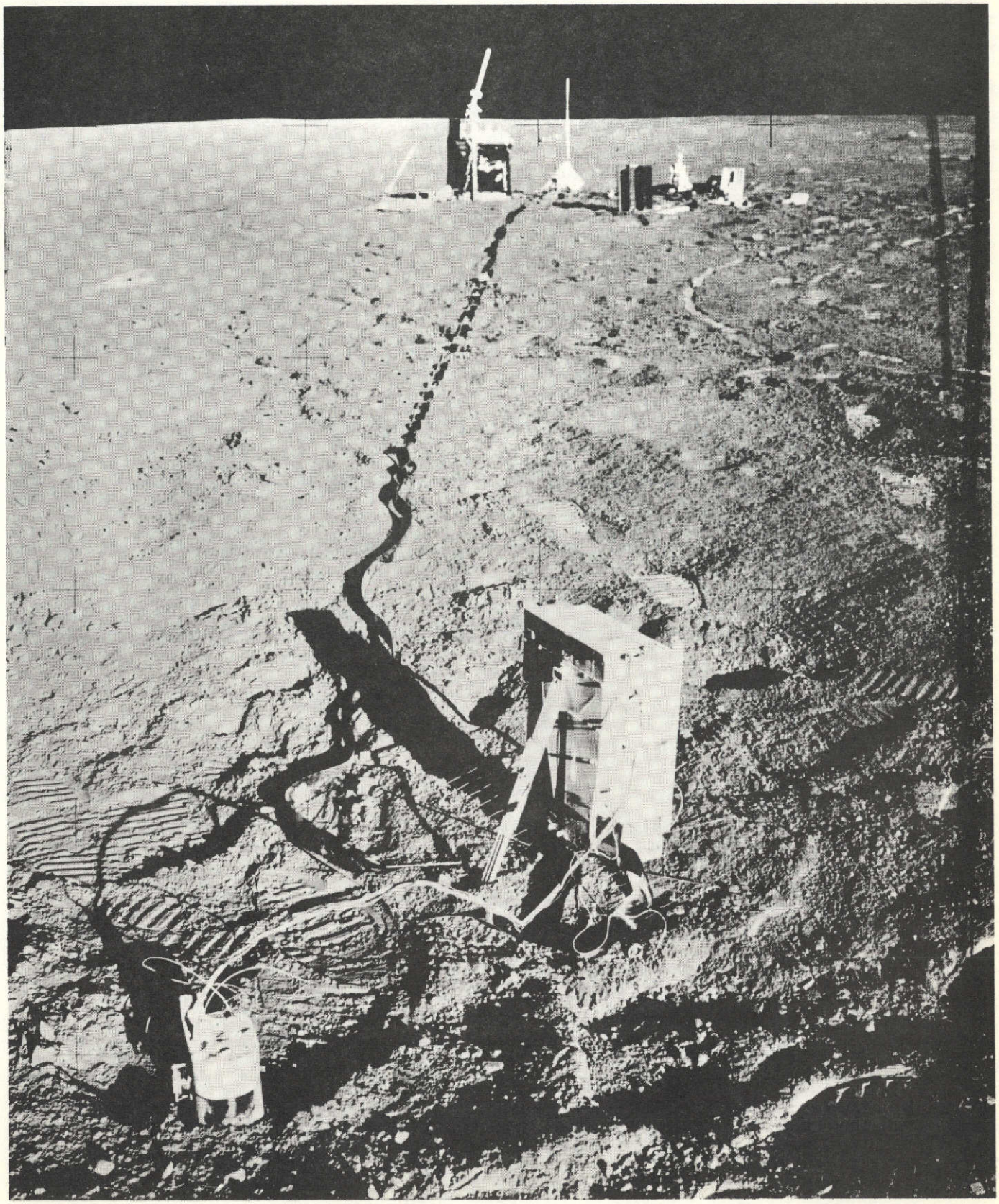

Figure 11 Cold cathode gauge as deployed on lunar surface during Apollo 14.

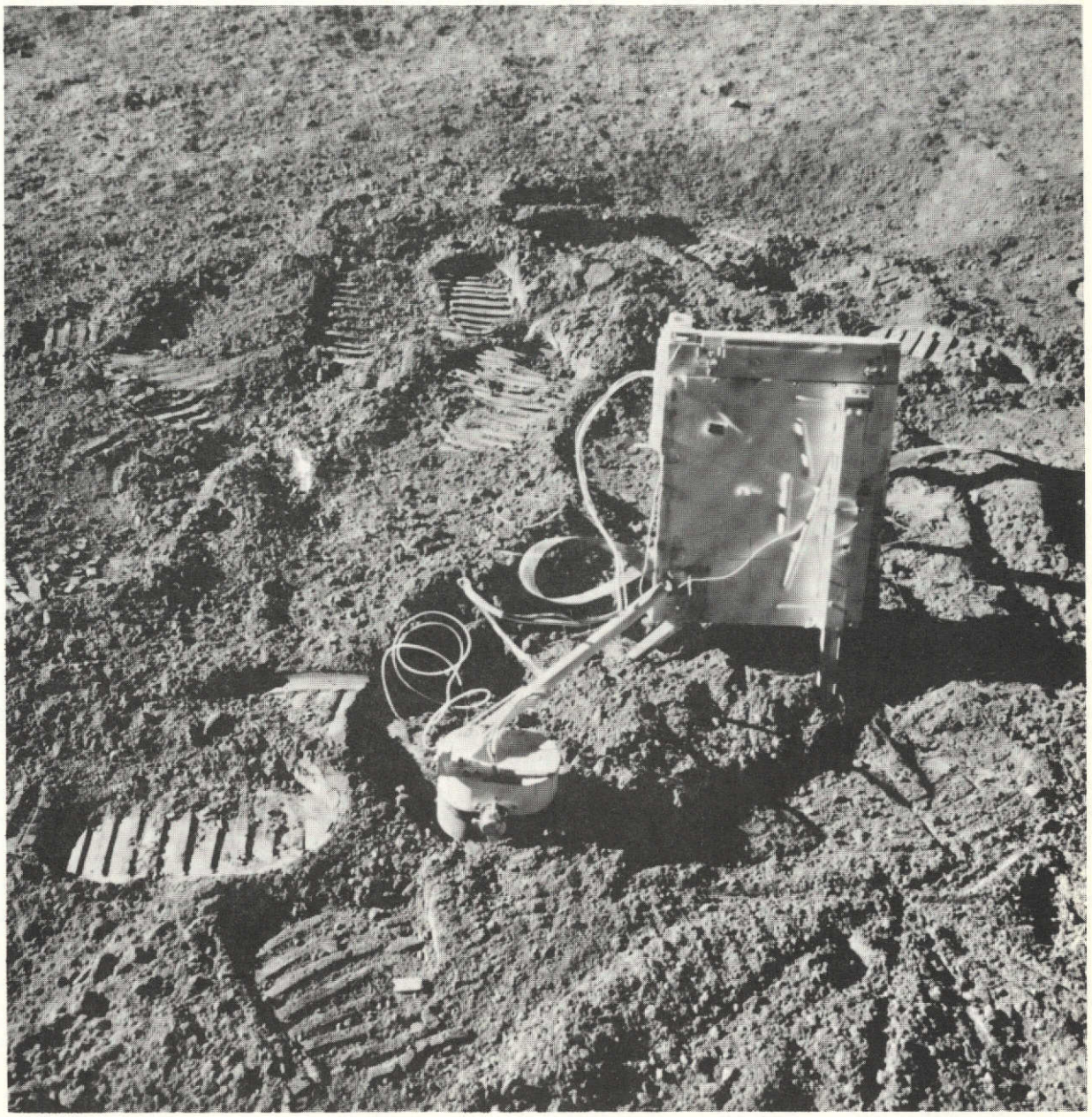

Figure 12 Cold cathode gauge as deployed on lunar surface during Apollo 15.

on the Apollo 15 experiment in that it allowed the tilt angle of the SIDE to be preset for optimum operation at the latitude of the chosen landing site. The deployment for Apollo 15 was much less trouble for the astronaut owing to the elimination of the cable problems encountered in the Apollo 12 and 14 deployments.

OPERATIONAL HISTORY

Apollo 12

The Apollo 12 Cold Cathode Ionization Gauge was turned on at approximately 2000 GMT on 19 November 1969, and a full-scale response was obtained due to gases trapped within the gauge. After about 1/2 hour, the response changed perceptibly from the full scale reading. After 7 hours, the indicated gas density was about 3.2×10^{14} m^{-3}. On lunar module depressurization prior to the second EVA, the response rose to at least 2.0×10^{15}, the exact value was in doubt because a calibration cycle occurred at the time of maximum pressure indication and obscured the readings. The increase in pressure at the gauge as a result of release of gas from the lunar module is in reasonable agreement with expectation. However, the loss of data near the peak of the pressure pulse eliminated any prospect of making meaningful diffusion studies based on the data.

During the second EVA, the response went off scale as Astronaut Pete Conrad approached the gauge, due to gases released from his life support system. Figure 13 shows the response. Again, the response is in agreement with expectation. No close comparison with prediction can be made due to lack of quantitative information on the separation between the astronaut and the gauge.

A catastrophic failure occurred after about 14 hours operation; the 4500 volt power supply went off. Two possibilities exist on this: (1) there may have been a failure, such as a short circuit, in the high voltage supply; (2) the toggle command may have failed, for its failure mode was such as to turn off the high voltage. There is no way of discriminating between these two possibilities, but the latter appears to be the more likely. In testing and development no failures were encountered with the high voltage supply. However, logic failures did occur brought about as a result of arcing when testing the package under inadequate vacuum. It appears that this failure may have been brought about by arcing following gassing within the electronics package as the package heated up on the lunar surface.

The problem was discussed at a meeting at Rice University December 11, 1969. It was agreed that both high voltage power supplies (the +4500 volt supply for the CCGE and the -3500 volt supply for the SIDE) would be left off for a longer period of time following deployment to allow more time for degassing of the electronics package.

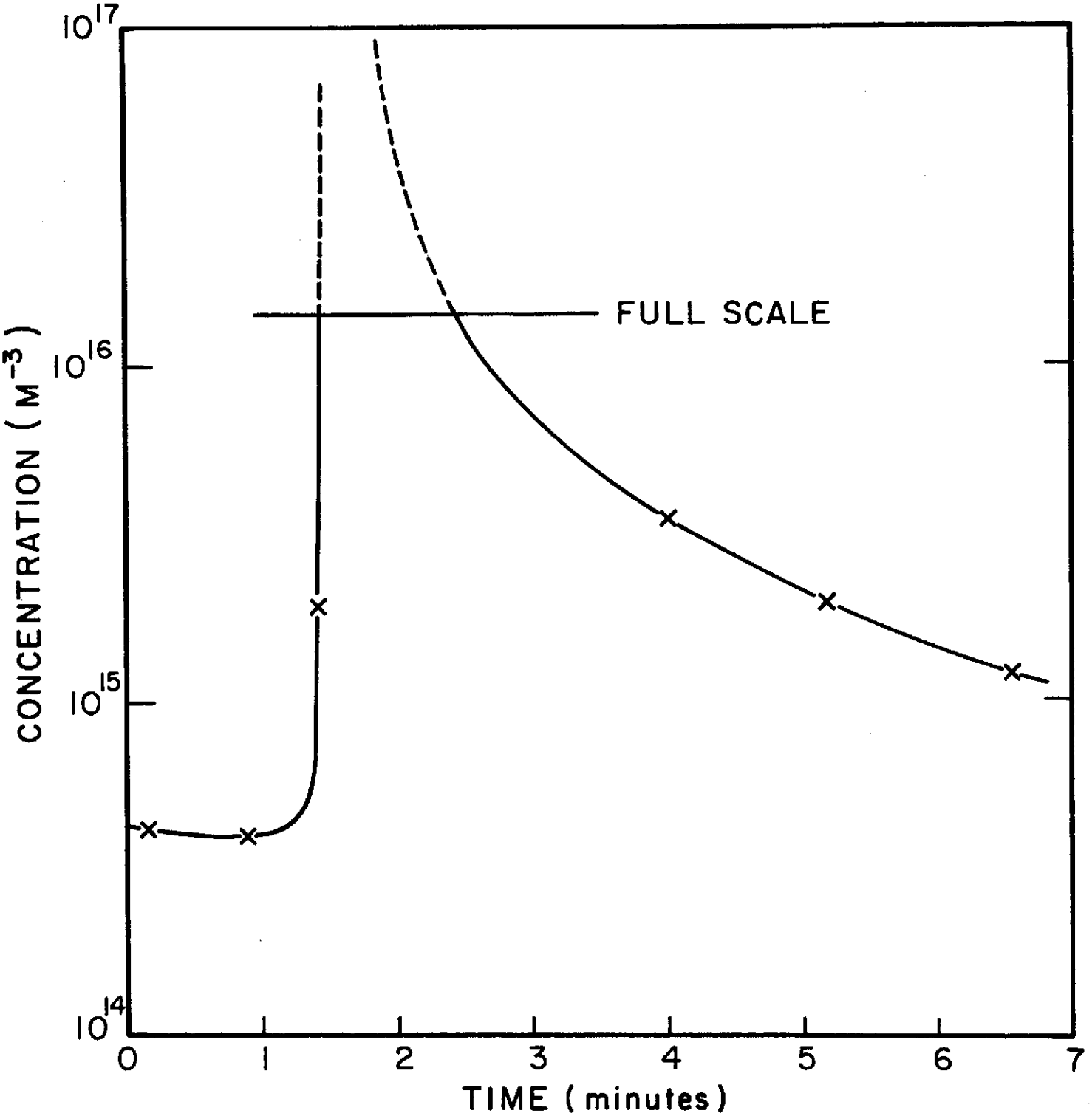

Figure 13 Effect of astronaut approaching gauge during Apollo 12.

Apollo 14

The Apollo 14 instrument was first activated on February 6, 1971 while the astronauts were still on the lunar surface. The unit was operated for short periods of time (approximately 30 minutes at a time) during the lunar module venting for the 2nd and 3rd EVA's. The experi- was then turned off until lunar sunset as a precaution against possible high voltage arcing problems as the electronics heated up during the lunar day and degassed.

During the next several months, the instrument was not activated during the lunar daytime except for brief periods in order to allow the package to outgas and so to minimize the possibility of high voltage arcing. Table 5 shows the approximate times of operation. The period of operation was increased each month until complete operation was obtained during the daytime by November 1971.

In April 1971, the positive analogue-to-digital converter became erratic, operating properly only intermittently. Soon thereafter, the converter became completely inoperative. This problem was not serious as far as the CCGE data were concerned, since it affected only the temperature and housekeeping data.

No additional problems other than occasionally noisy data were encountered with the CCGE until the nighttime operation in February of 1972. At that point the CCGE data dropped out for about four days at the end of the lunar night, but they came back at sunrise. This problem

TABLE 5

Apollo 14

Data Available at NSSDC

From Day/Hour/Minute/GMT		TO
1971		
37/00/51	Spot Operation	37/13/40
50/16/30		66/21/00
77/14/00		97/10/44
107/12/15		128/14/15
135/13/00		157/23/40
159/12/00		159/14/00
165/13/00		187/19/10
194/14/44		217/10/44
217/21/00	Spot Operation	219/09/00
223/21/00		232/17/46
236/17/44		246/05/44
253/22/15		275/20/30
276/16/30	Spot Operation	281/19/55
282/15/45		311/00/44
312/17/44		365/23/59
1972		
000/00/08		009/00/00
009/17/44		068/17/44
069/17/44		177/06/44
179/17/44		205/06/30
207/14/44		271/12/50
275/17/44		307/17/44
311/17/44		346/22/50
351/17/44		365/23/59
1973		
000/00/00		132/00/00

occurred intermittently until the nighttime operation in late November 1972, at which time all nighttime data were lost. This complete loss of nighttime data lasted for two months, followed by one month of complete data acquisition in late March 1973, and then two more months with no nighttime data.

The start of the lunar day on April 15, 1973 produced the third and the most serious problem. At this time the SIDE/CCGE went into the standby condition (high voltage supplies turned off), and no data were available from either the SIDE or CCGE. Attempts to restore the experiment to normal operation were unsuccessful until the following lunar night, at which time the CCGE high voltage was restored but the SIDE high voltage had to be left off. In this condition, the CCGE nighttime data were again good and remained good until an unsuccessful attempt was made about sunrise to restore the SIDE high voltage. After sunrise it was not possible to obtain operation with either of the high voltages on, and the experiments were left in standby until sunset. There was no successful daytime operation after April 15, 1973, and the nighttime operation was only intermittently successful.

Apollo 15

The Apollo 15 cold cathode gauge was operated only for short time periods after deployment and original turn-on on July 30, 1971. The operating times coincided with the depressurization times of the

lunar module for the various EVA's and with the lift-off time of the accent stage of the lunar module. Following the brief period of operation near lift-off, the unit was turned on at about 0253 GMT August 3, 1971 for another short period. The instrument amplifier was left on in order to monitor temperature, but the high-voltage supply was off to prevent the possibility of arcing within the package as it heated up and degassed. Table 6 shows the approximate times of operation of the Apollo 15 instrument.

The high voltage supply was turned on at approximately 0130 GMT August 13, 1971 and remained on until about 0952 GMT August 30, 1971. During this period of time several increases in concentration were observed apparently due to release of gas from various hardware items left on the lunar surface. The high voltage was turned off during most of the lunar day time for the first few months to minimize the possibility of arcing. However, when the voltage was turned off at about 0500 GMT, September 28, 1971, a low value of leakage current appeared and continued to be present from that point on. This leakage current appears on the plot as a very low concentration during the daytime records where the high voltage was off.

The Apollo 15 CCGE operation was good until February, 1973, at which time the nighttime data became eratic. During the problem periods, the data appear very noisy and are probably completely meaningless; the automatic zero and calibration functions do not operate

TABLE 6

Apollo 15

Data Available at NSSDC

1971			
	212/18/56	Original turn on and spot operation	215/02/53
	225/01/30		242/09/52
	253/16/30		271/05/40
	271/05/40	Spot Operation	282/15/53
	282/15/53		302/23/20
	302/23/20	Spot Operation	312/13/02
	312/13/02		336/13/10
	341/16/52		352/18/52
	356/18/52		364/15/30
1972			
	004/18/52		030/13/52
	034/14/00		057/18/52
	058/12/52	Spot Operation	063/14/00
	063/14/00		006/18/52
	087/18/52		088/16/10
	092/14/52		118/01/20
	122/21/40		148/04/10
	149/05/00		190/02/30
	191/18/52		194/03/00
	195/18/52		263/23/52
	267/18/52		365/23/59
1973			
	000/00/00		228/00/00

properly. This problem also occurred during daytime operation starting in August 1973 and no data are available past that date. It probably involves a complete failure in instrument logic.

Anomalies

Several anomalies in the data for both the Apollo 14 and Apollo 15 experiments have occurred. Some of the anomalies cannot be explained but most have been traced to noise originating either in the gauge or the electronics.

Both experiments experienced noisy data during sunrise and sunset when the package temperature was changing rapidly. One example is shown in Figure 14 for the Apollo 15. The noisy period near sunrise extended over a 3 or 4 day period for Apollo 14.

Figure 15, showing Apollo 14 data, is a good example of two other anomalies which occurred on both of the experiments. The noisy data at the beginning of the plot is caused by the gauge operating in a range where oscillation occurs (refer to section on calibration at MRI). Both gauges experienced the oscillation at repeatable density levels.

The other anomalies shown in Figure 15 is the abrupt drop in density near the middle of the plot. This is caused by the gauge discharge mode change characteristics, and also repeats at the same density level every time.

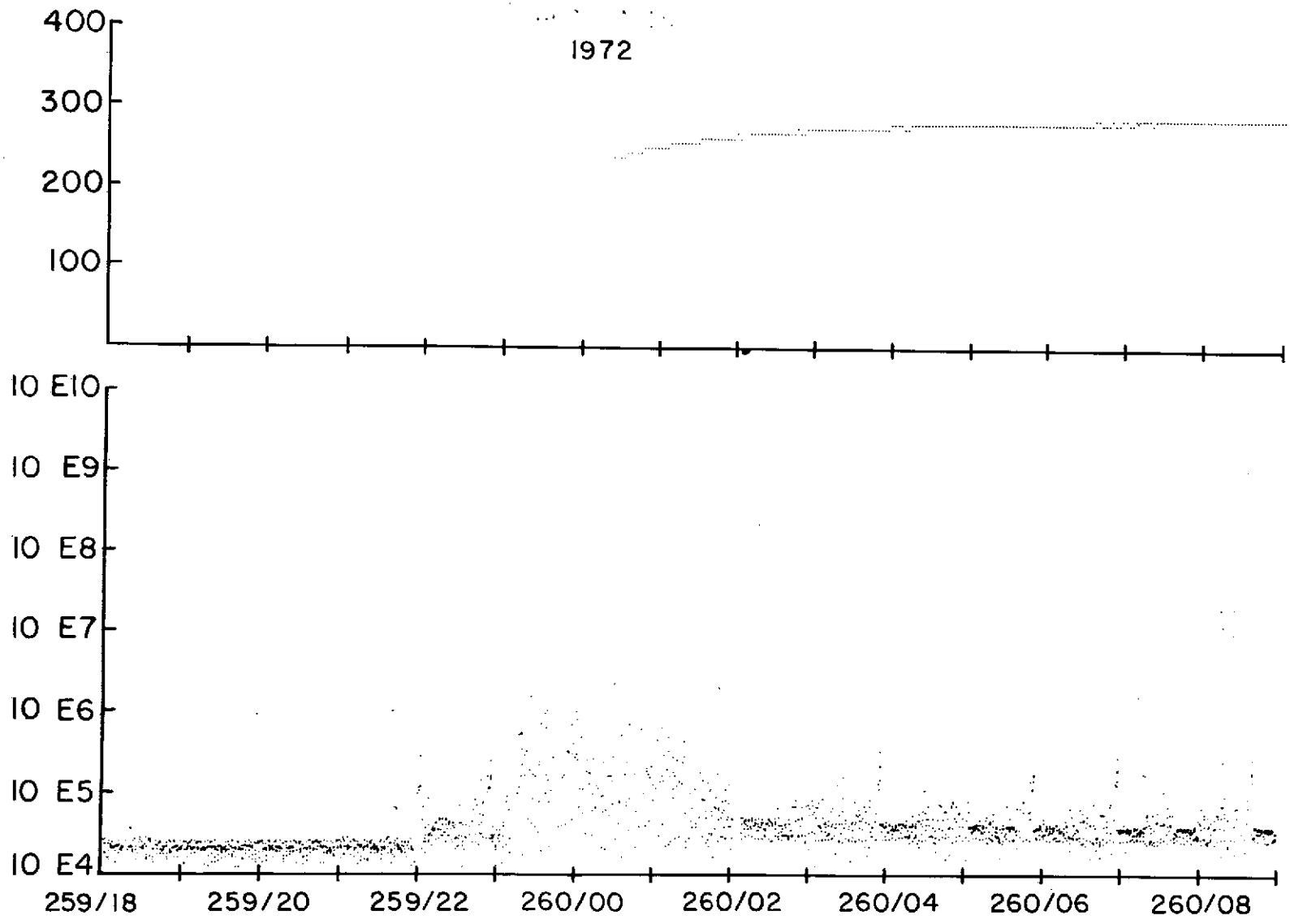

Figure 14 Temperature rise of gauge at Apollo 15 site (upper panel) and noise response of gauge at sunrise. The abcissa scale is day of year/hour GMT. The ordinate scales are degrees K and concentration in particles per cubic centimeter.

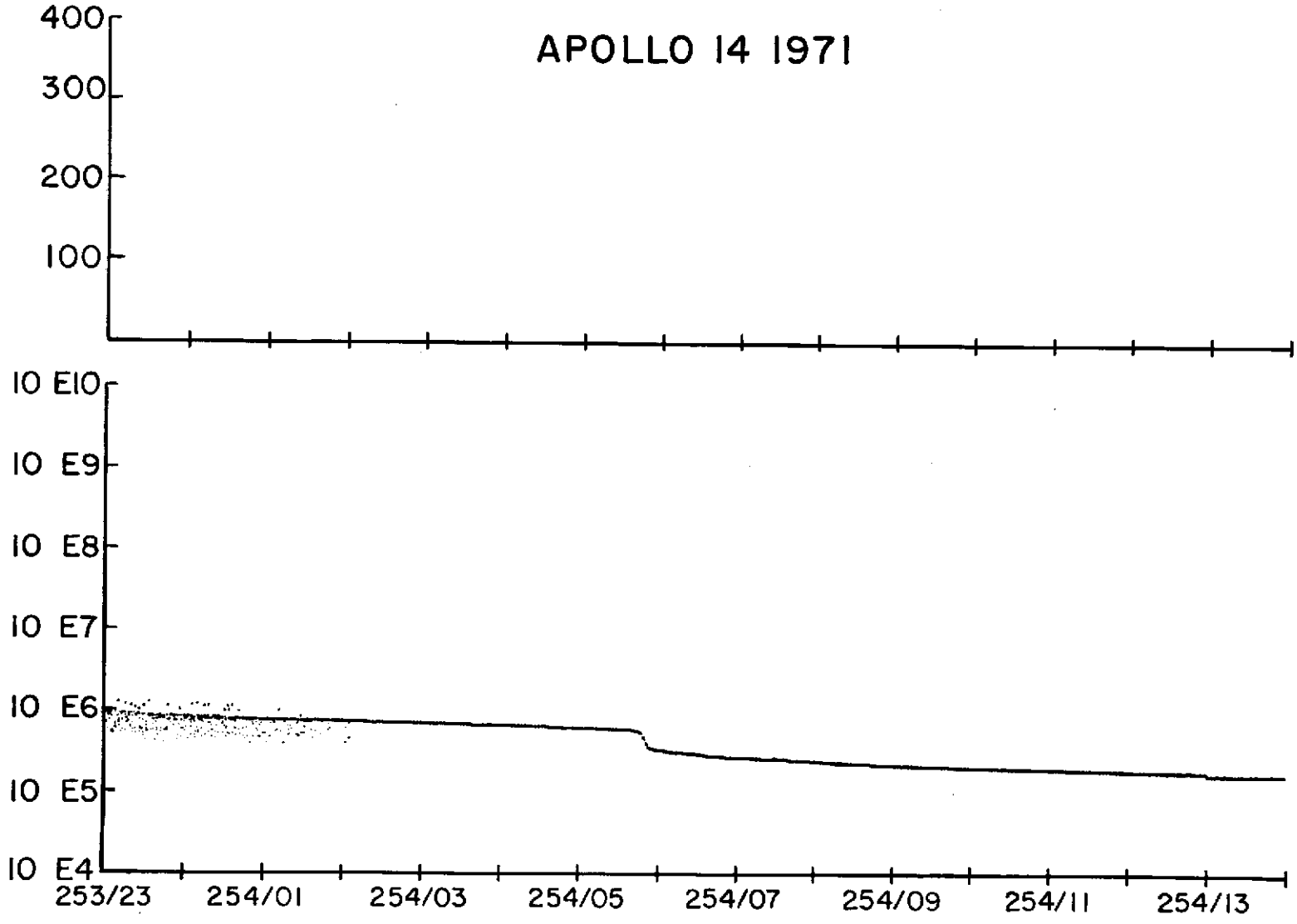

Figure 15 Portion of Apollo 14 record showing noisy response due to electrical oscillation in gauge and sudden change in response due to change in discharge made within gauge.

Figure 16 shows the same two anomalies for the Apollo 15 experiment but with the density increasing. The magnitude of gauge oscillation is not as large in Figure 16 as in Figure 15.

Figure 17 shows an anomaly which occurred in the Apollo 15 data. The double trace is caused by crosstalk within the SIDE electronics package and occurred intermittently. The crosstalk occurred in the data transmitted in particular SIDE frames or data words.

RESULTS

The results of the Cold Cathode Gauge Experiment are summarized in Figures 18 and 19 for Apollos 14 and 15 respectively. The nighttime concentrations were observed to be unvarying and near 2×10^{11} particles m^{-3}, corresponding to 10^{-12} torr at 100 K. This is in good agreement with the neon concentration expected from the solar wind source. The contaminant gases from the Apollo operations, and perhaps some ambient lunar gases as well, are very completely adsorbed on the lunar surface at night, and hence they do not show up in the nighttime observations.

The observed daytime concentrations were much greater, and they generally decreased from month to month. The temperature history of the gauges repeated itself month after month (except for perturbations associated with eclipses), and the temperature patterns are also shown

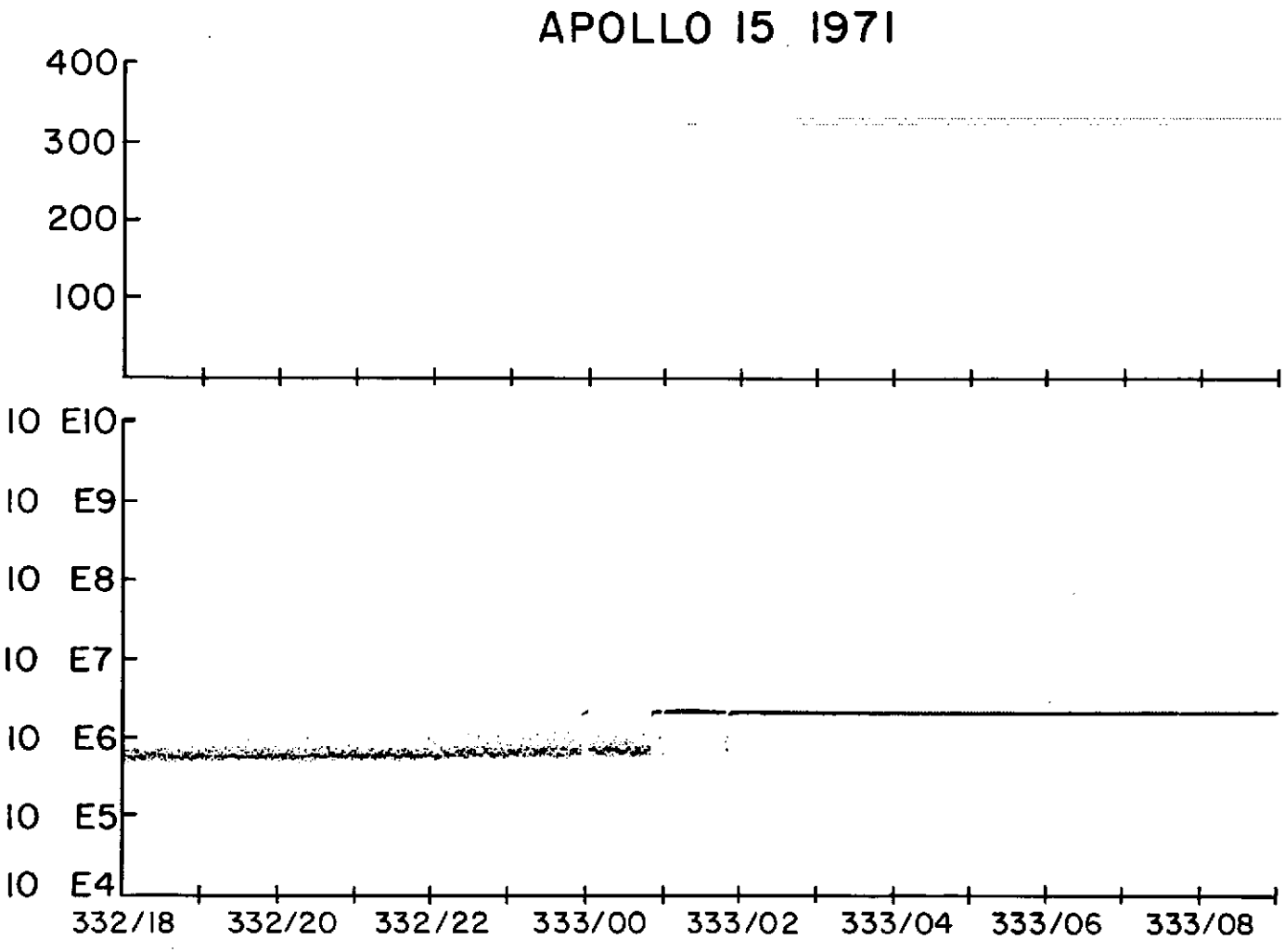

Figure 16 Portion of Apollo 15 record showing noisy response due to electrical oscillation in gauge and sudden change in response due to change in discharge mode within gauge.

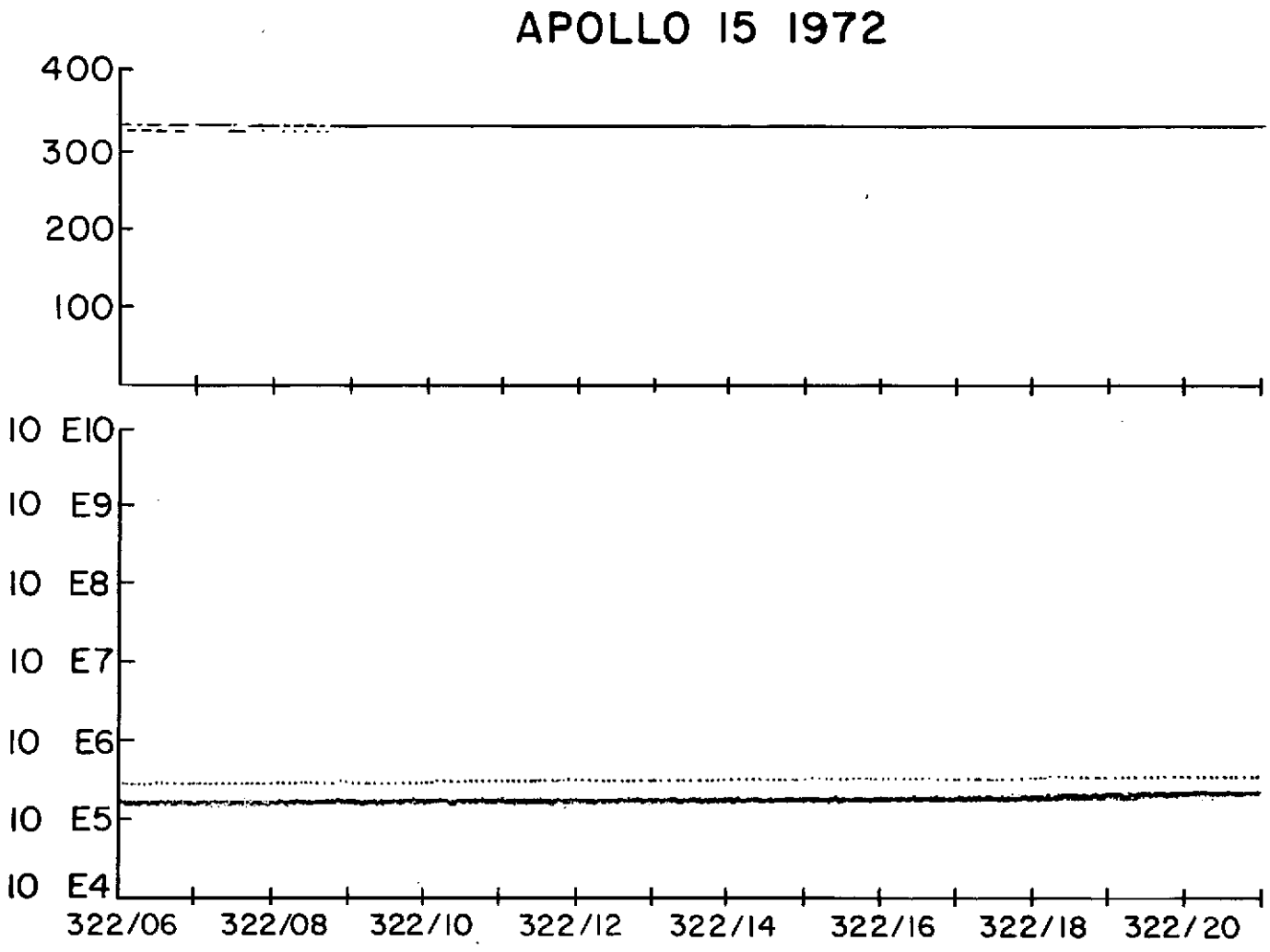

Figure 17 Portion of Apollo 15 record showing effect of crosstalk on one data frame appearing as a separate trace.

in Figures 18 and 19. On both gauges, the temperature rose very rapidly at sunrise from 100 K to 250 K within a few hours and then increased slowly to a flat peak near midday. The temperature history for Apollo 14 was nearly symmetric about midday; the temperature maximum occurred about 10 hours after midday. The temperature history for Apollo 15 was less symmetric, and the maximum was reached about 27 hours before midday. The temperature at sunset was about 270 K for Apollo 14 and 245 K for Apollo 15. After sunset the temperature fell rapidly to about 115 K one day after sunset and then slowly to about 100 K just before sunrise.

The concentration curves in Figures 18 and 19 are labelled with the number of the lunar day (lunation) starting with 1 as the day of the Apollo landing. Data are lacking through the hot part of the day for the first eight or ten days, as the gauges were not operated because of concern about possible arcing problems. The following points are evident from the curves: the daytime concentrations fell from month to month in a fairly regular pattern; the concentrations were very responsive to temperature near midday, changing by an order of magnitude for a temperature change of a few tens of degrees; and the maximum daytime concentrations seemed to stabilize at values near 7×10^{12} particles m^{-3} at the Apollo 14 site and 3×10^{12} at the Apollo 15 site. This latter point is further illustrated in Figures 20 and 21, which show the midday concentrations at the Apollo 14 and 15 sites respectively over the lifetimes of the CCGE's.

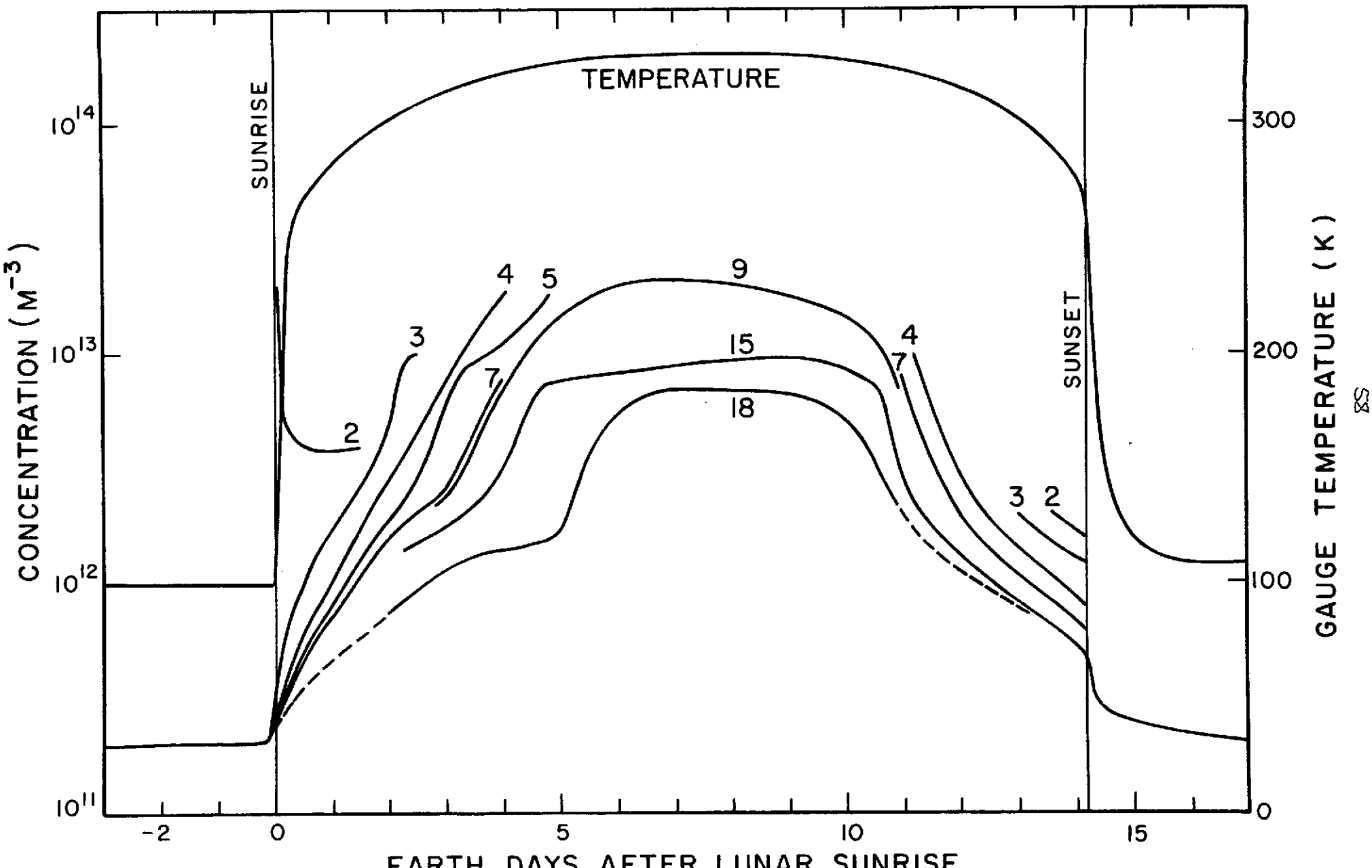

Figure 18 Gauge temperature history through lunar day for Apollo 14 and concentration curves for selected lunar days. Lunar day 1 is day of landing, and following lunar days are numbered in sequence.

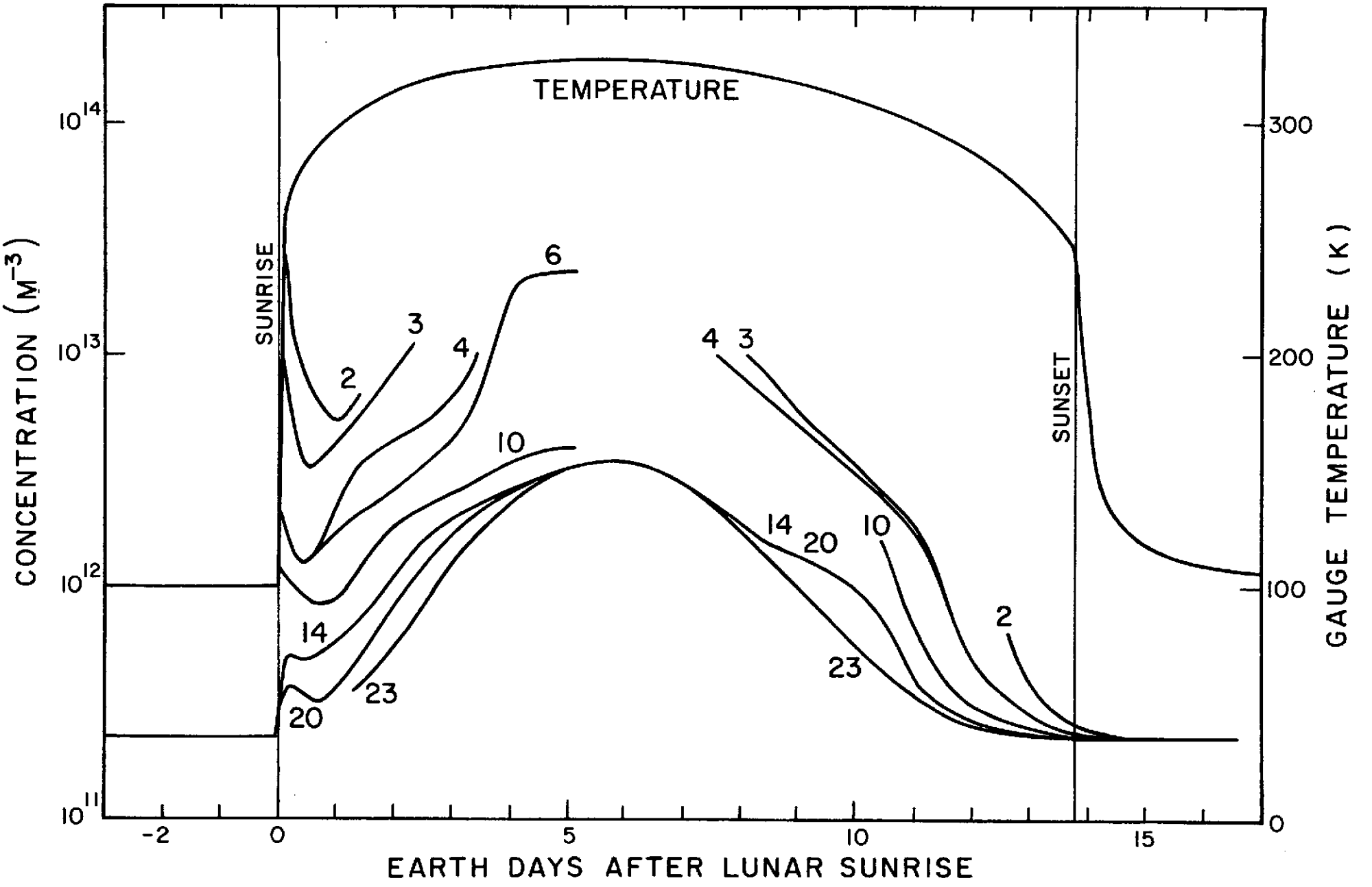

Figure 19 Gauge temperature history through lunar day for Apollo 15 and concentration curves for selected lunar days. Lunar day 1 is day of landing, and following lunar days are numbered in sequence.

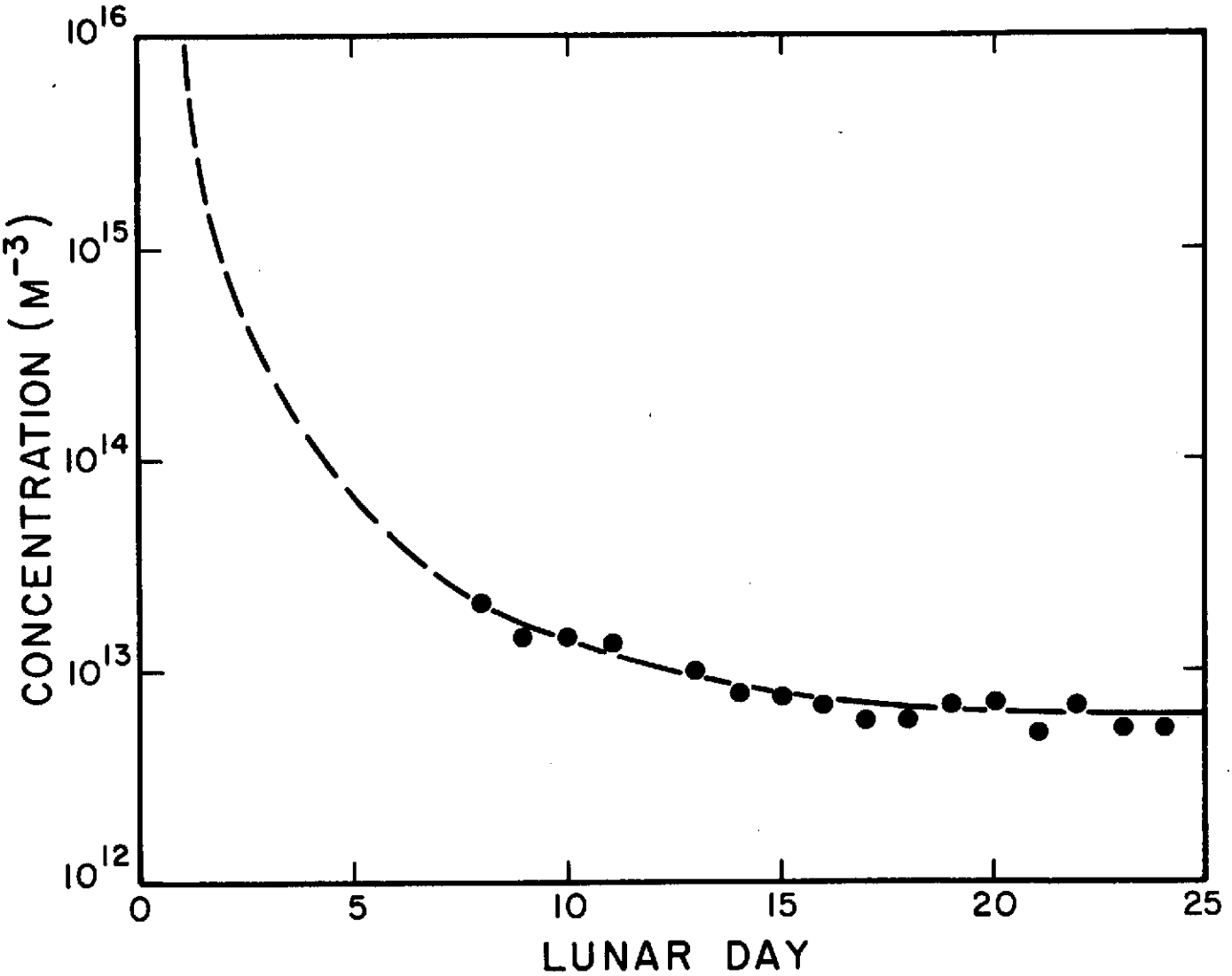

Figure 20 Concentrations near lunar midday for succession of days observed by Apollo 14 CCGE.

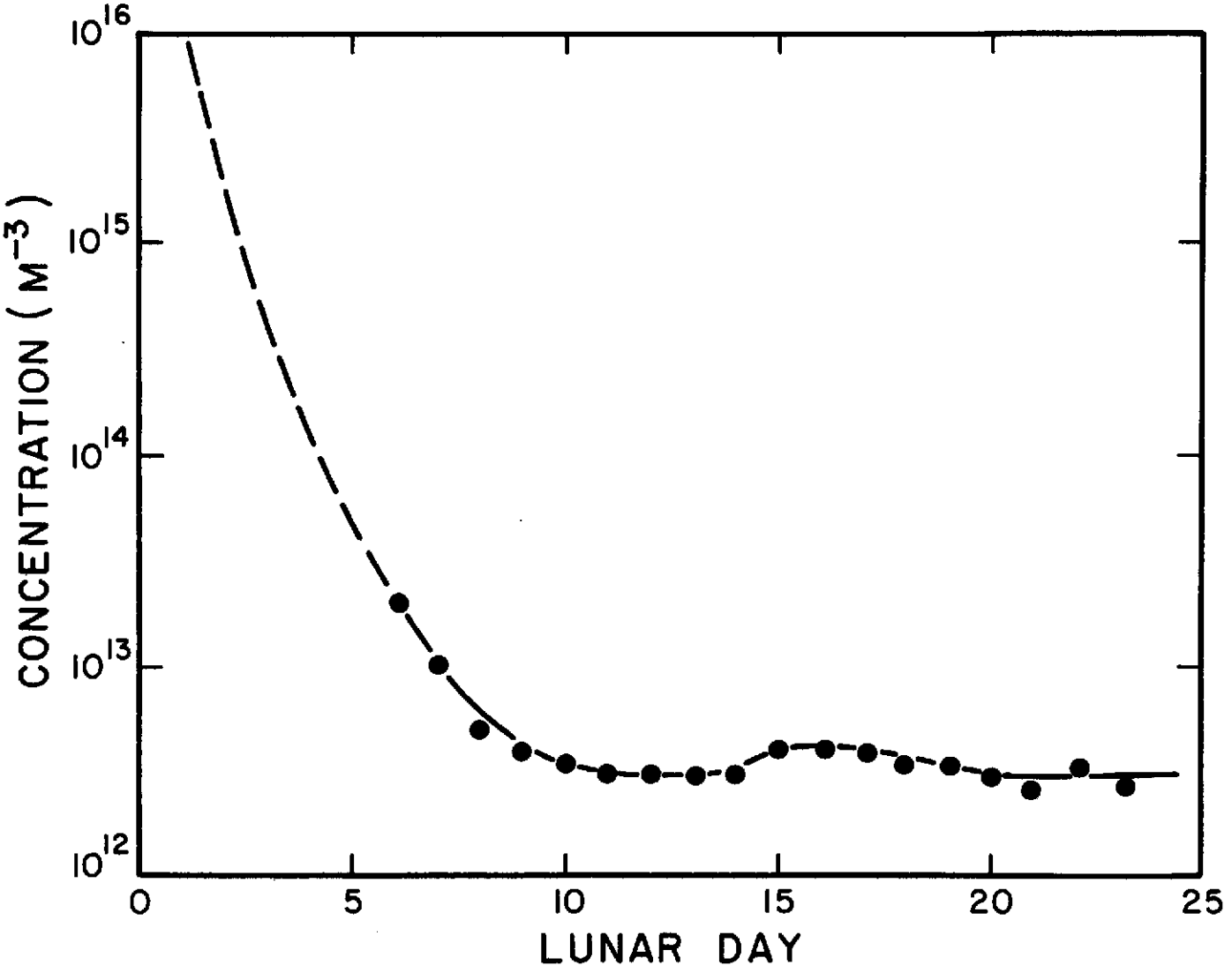

Figure 21 Concentrations near lunar midday for succession of days observed by Apollo 15 CCGE.

Sunrise Effect

A pronounced peak in concentration occurred a few hours after the first sunrise on Apollo 14 (lunar day 2), as can be seen with very poor time resolution in Figure 18. Similar peaks were not seen on subsequent sunrises. However, the response of the Apollo 14 CCGE was very noisy for a period of several days around sunrise, so small peaks could have occurred and escaped detection. Figure 19 shows a similar peak for Apollo 15, but in this case the sunrise peak prevailed through all subsequent sunrises, although it became small after a year. These peaks on Apollo 14 and Apollo 15 for the first year were undoubtably due to contaminants released from the spacecraft at night becoming adsorbed on the nearby lunar surface and released at sunrise. It is notable that the release occurred very rapidly, before the lunar surface had time to warm up very much. The release was probably a photo-release, stimulated by light quanta rather than by thermal energy.

Figure 22 shows the concentration at the Apollo 14 site at the first sunrise in more detail. The rise started before sunrise at the gauge and reached its maximum value by the time the sun was fully in view from the gauge. As the gauge and surroundings became warmer, the concentration fell. Figure 23 shows a similar curve for Apollo 15. Except for some structure near the peak, the result is almost identical with that from Apollo 14. Figure 24 in its lower half shows a super-position of several such curves for Apollo 15, and the gauge temperature

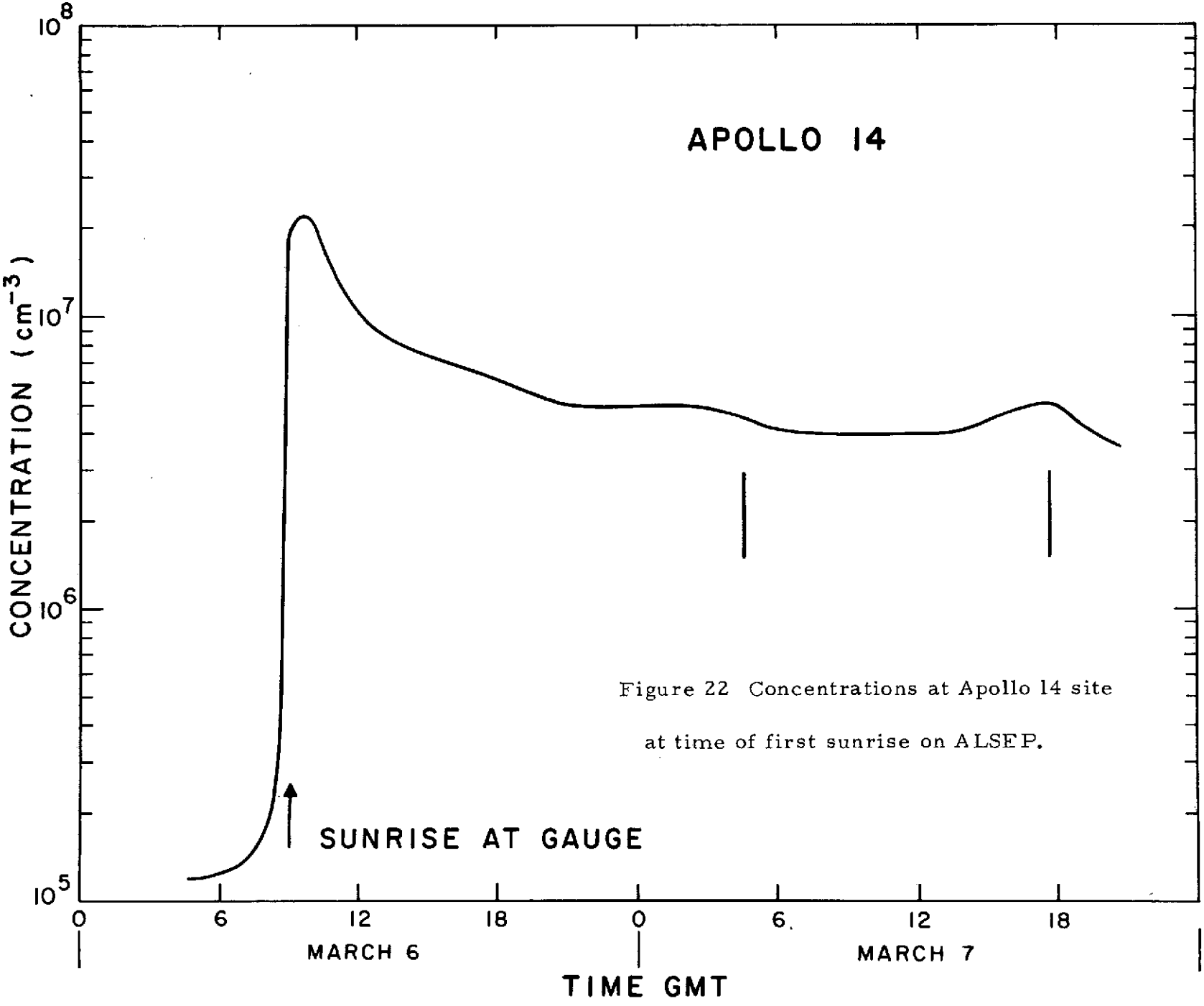

Figure 22 Concentrations at Apollo 14 site at time of first sunrise on ALSEP.

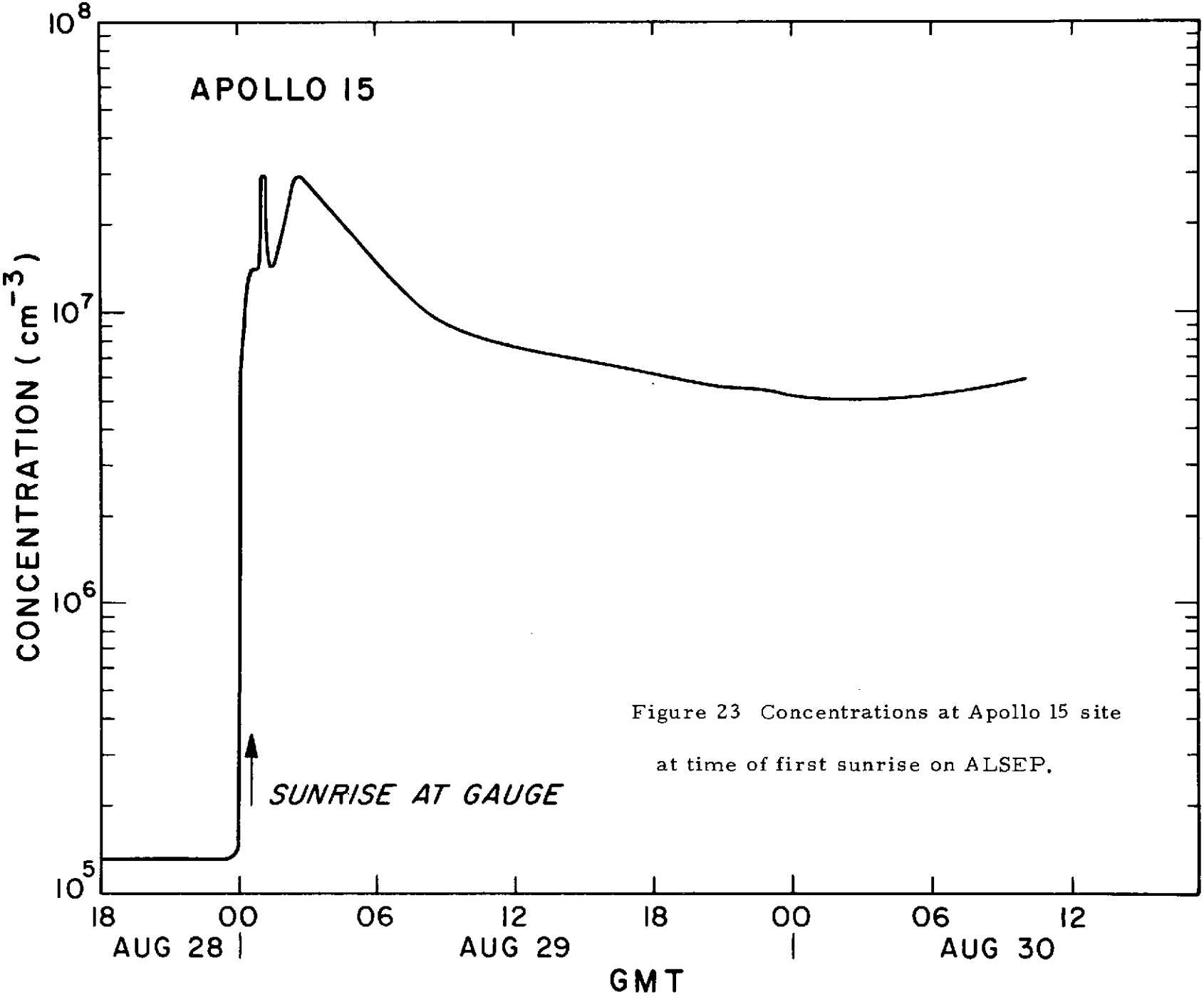

Figure 23 Concentrations at Apollo 15 site at time of first sunrise on ALSEP.

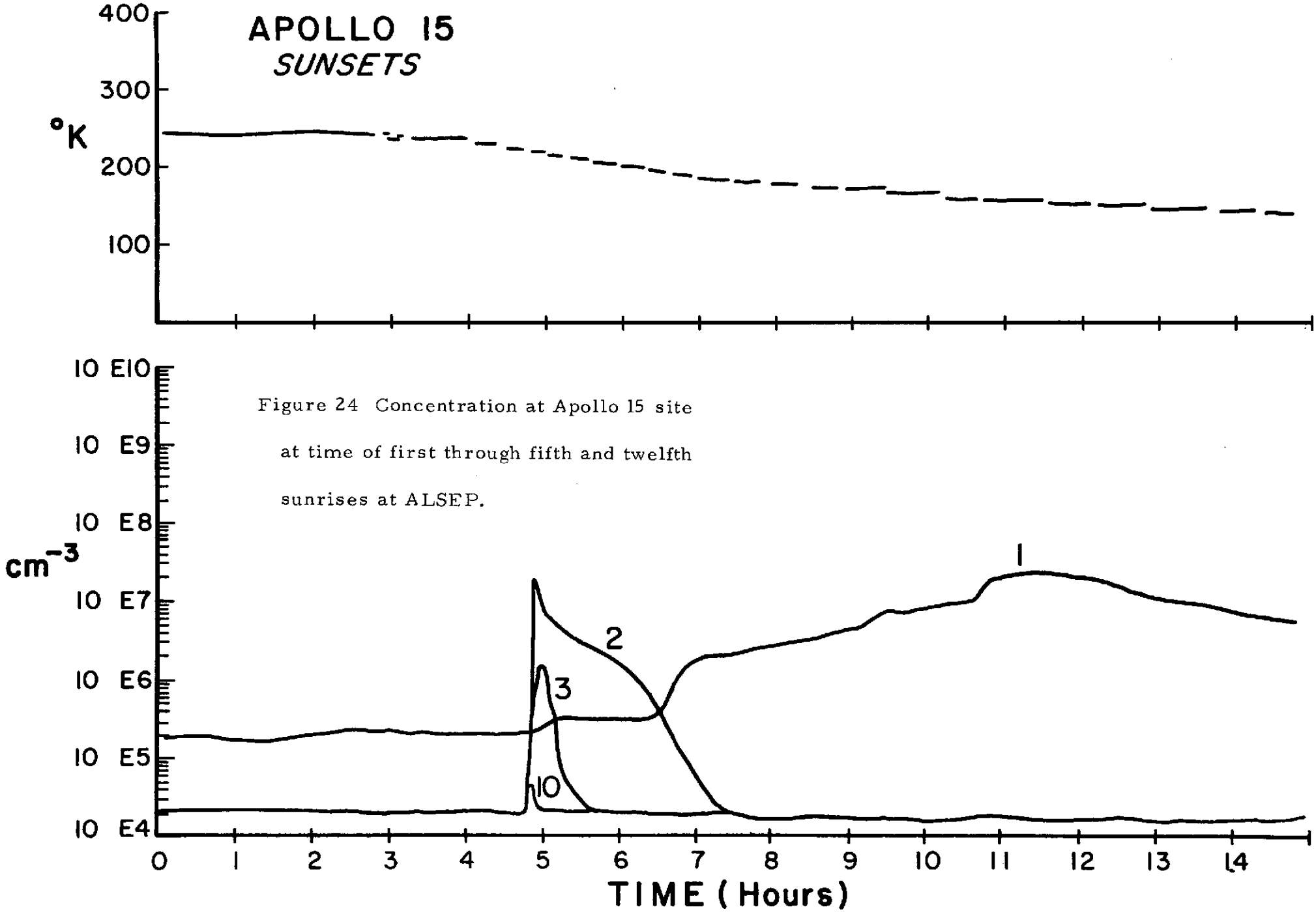

Figure 24 Concentration at Apollo 15 site at time of first through fifth and twelfth sunrises at ALSEP.

in its upper half. The concentration rise on the first and second lunar sunrises started about an hour before sunrise. The peak with later sunrises occurs as the gauge starts to warm up in the sunlight, and its time is probably to be associated with sunrise at the gauge. This also agrees with the narrow peak that appears in the structure at the peak in Figure 23. This short term (~1/2 hour) effect is probably associated with photorelease of gas adsorbed on the lunar surface near the gauge. What is not apparent in Figure 24 is that the concentration falls for almost a day after the sunrise peak while the lunar surface is warming.

The Lunar Module has proved to be an intermittent gas source, especially near the time of the first lunar sunset. Figure 25 shows conditions just after the first lunar sunset for Apollo 14. The concentration had reached the low value typical of lunar night when a sudden increase occurred that lasted for several days. Two small increases were superimposed on the big increase; these were at first thought possibly to be releases of gas from the lunar interior because their rise times were longer than those characteristic of impulsive releases of gas from the lunar module. However, the frequency of such events decreased with time, and it seems more reasonable to associate them with the LM than with the moon. Just after the first sunset on Apollo 15, a somewhat similar large release of gas occurred, less long lasting than on Apollo 14 but larger in magnitude, as shown in Figure 26. Two short bursts of gas followed that large increase, reminiscent of the two

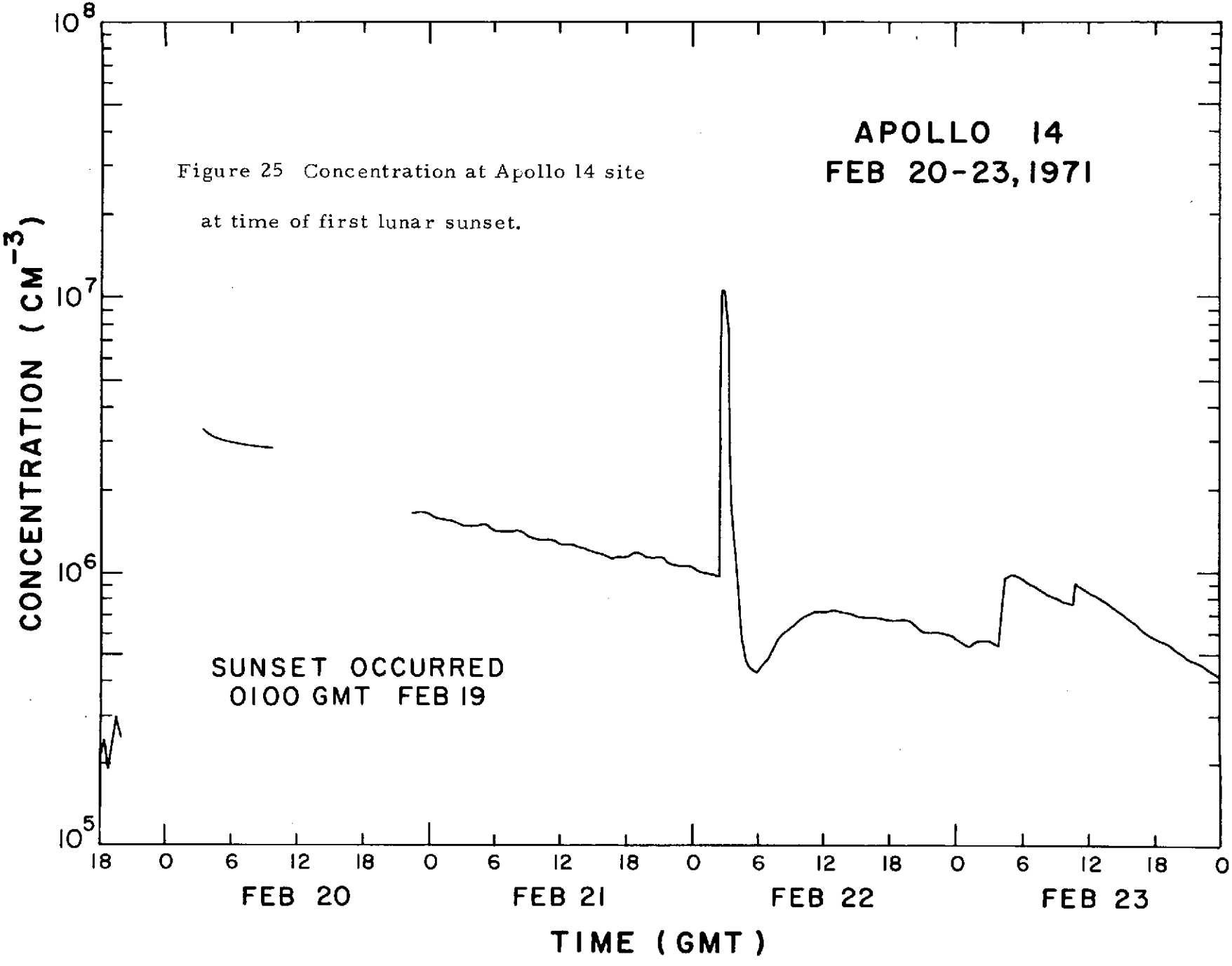

Figure 25 Concentration at Apollo 14 site at time of first lunar sunset.

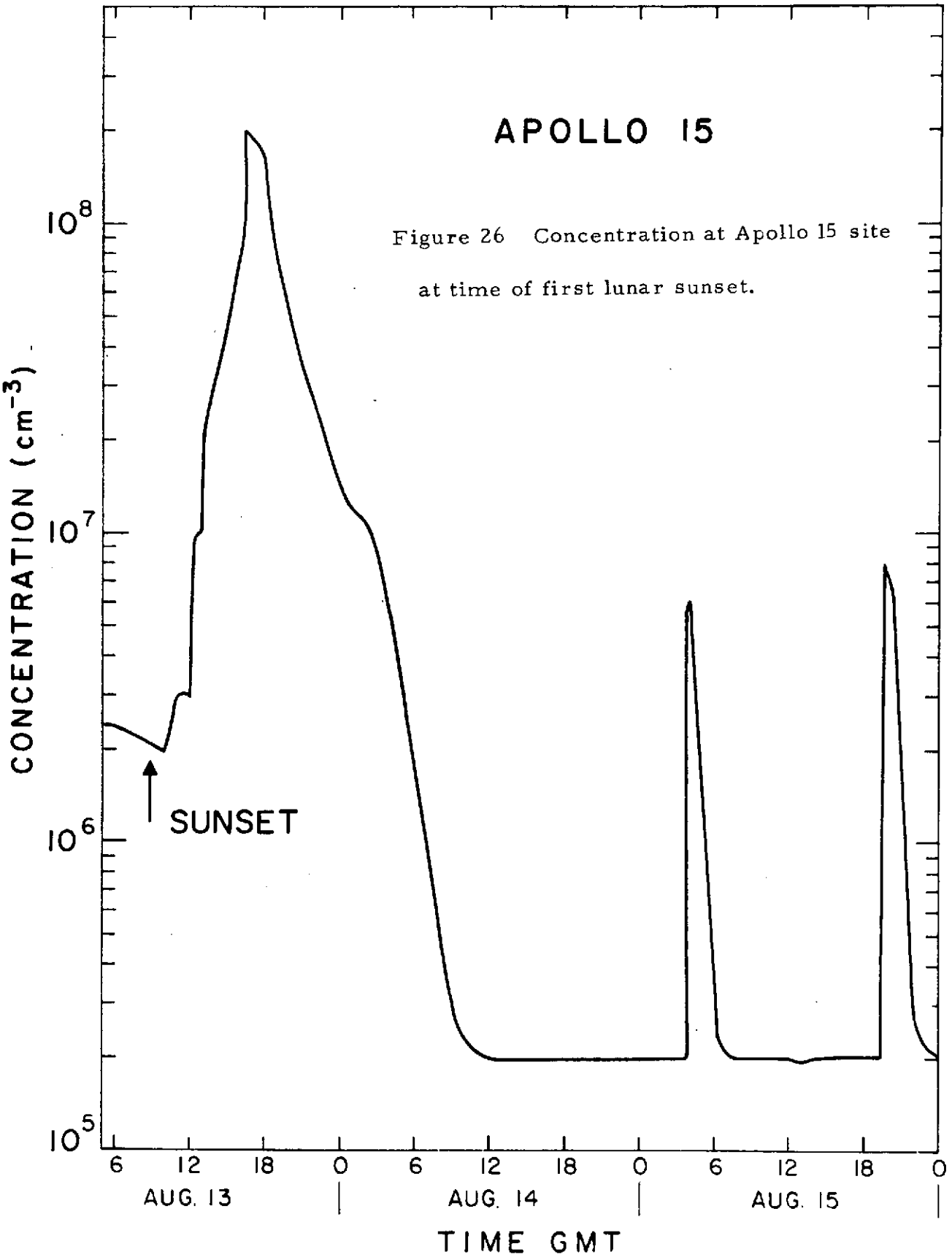

Figure 26 Concentration at Apollo 15 site at time of first lunar sunset.

small increases on Apollo 14. Apollo 15 exhibited a similar gas release at the time of its second lunar sunset, as shown in Figure 27.

Short bursts of gas occurred with amazing regularity on both Apollo 14 and Apollo 15, following each lunar sunset by about two hours. The effect persisted for at least eight months with slowly decreasing amplitude. The source of this recurrent burst is almost surely associated with the LM. Figure 28 shows the Apollo 15 sunset chracteristics for the 1st, 2nd, 3rd and 10th lunar sunsets.

Figure 29 shows the gauge response during the final depressurization of the Apollo 14 lunar ascent stage to discard unneeded hardware. The gas concentration rose sharply by about an order of magnitude as the depressurization valve was opened. However, the umbilical connection to Astronaut Shepherd's spacesuit was not latched and he began to experience depressurization, so the valve was closed and the pressure fell rapidly to its former value. This false start was followed by a second. The actual depressurization of the lunar module was completed on the third try. Some of the spikes near the end of the record shown in Figure 29 were associated with the observed impact of discarded life-support items striking the lunar surface.

One should note the rapid rises in concentration in Figure 29. The depressurization valve apparently opens very quickly, as the entire concentration rise takes place within the 2.4 second interval between readings. One could not expect such a rapid rise if the gas source

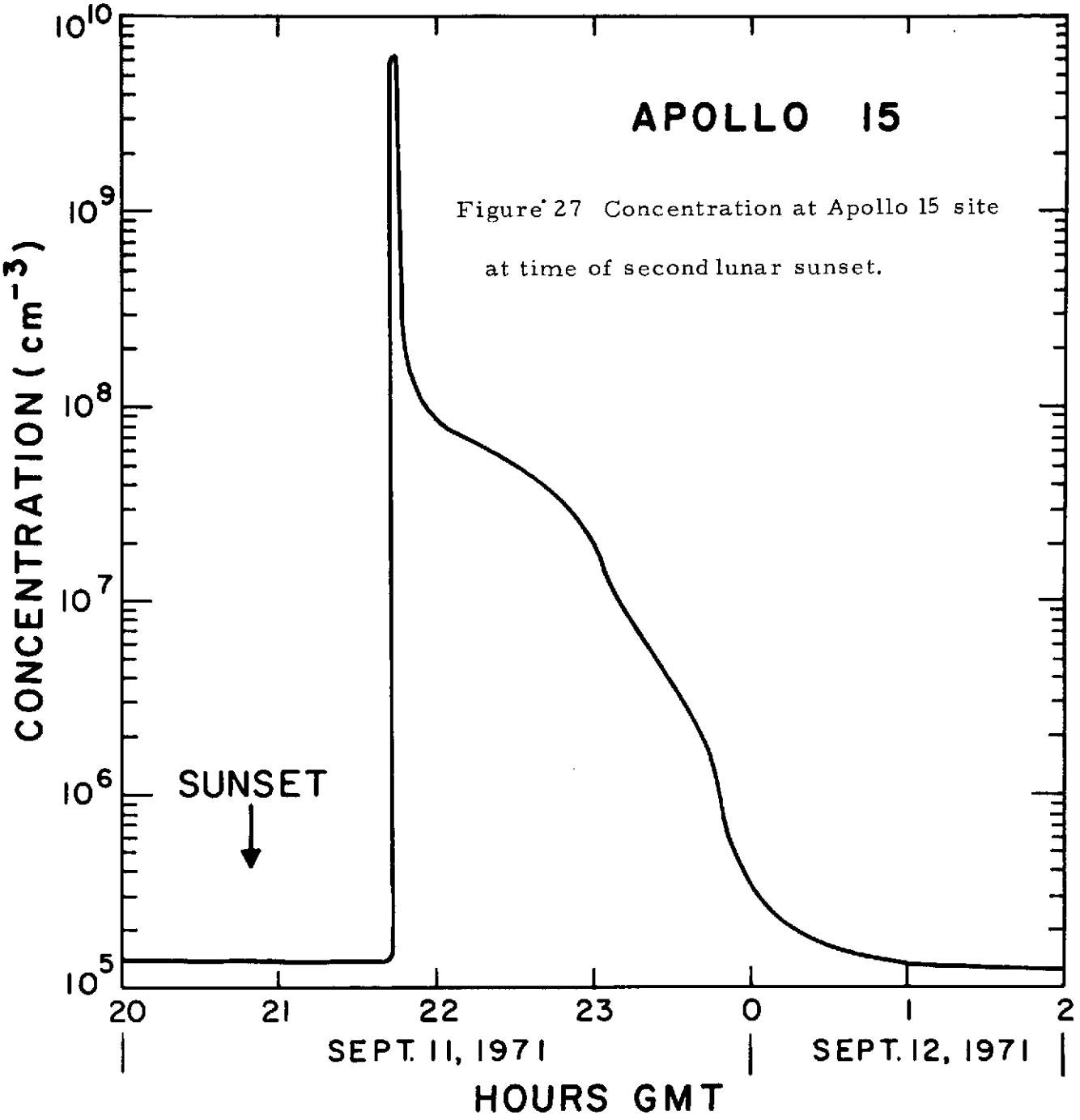

Figure 27 Concentration at Apollo 15 site at time of second lunar sunset.

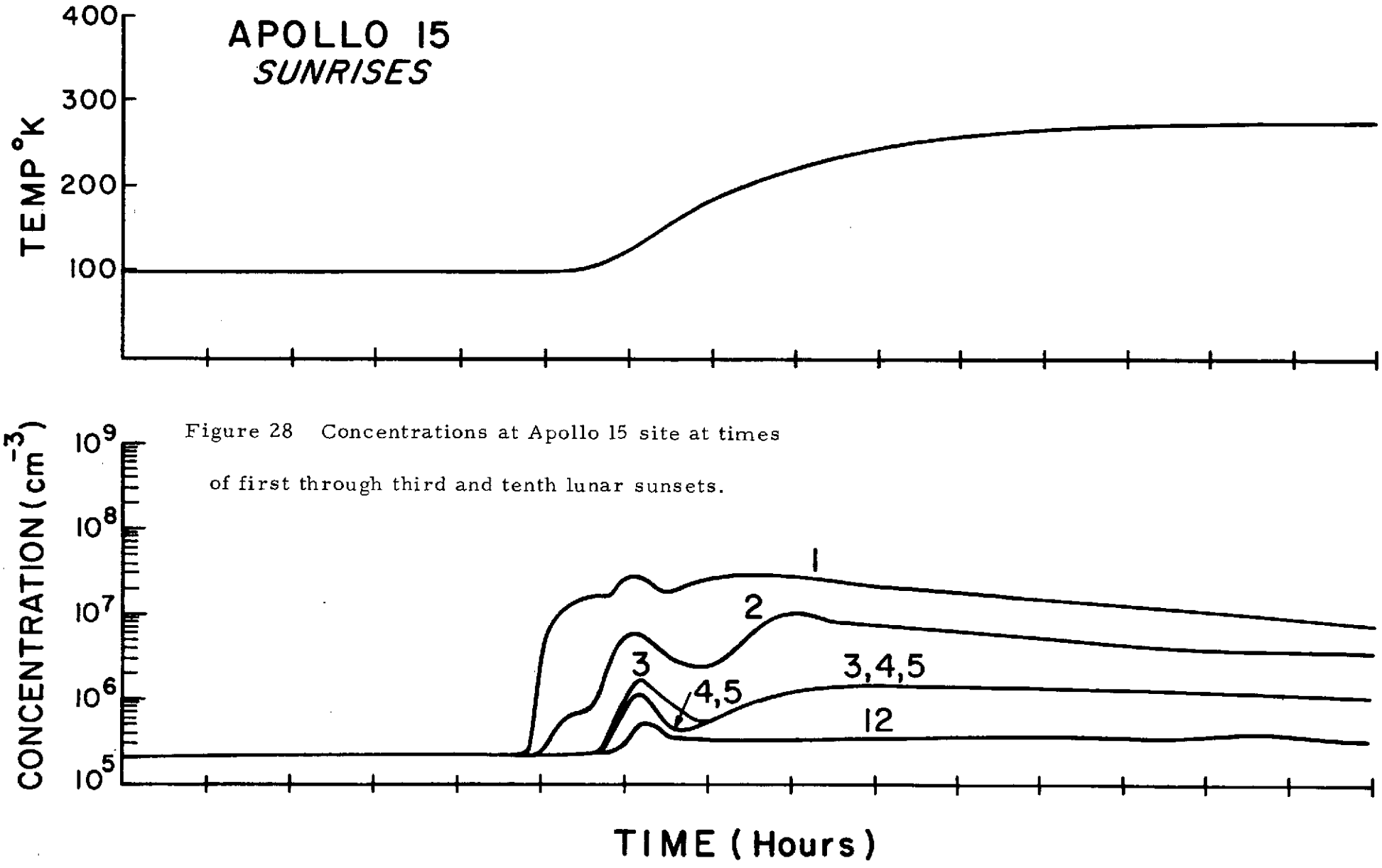

Figure 28 Concentrations at Apollo 15 site at times of first through third and tenth lunar sunsets.

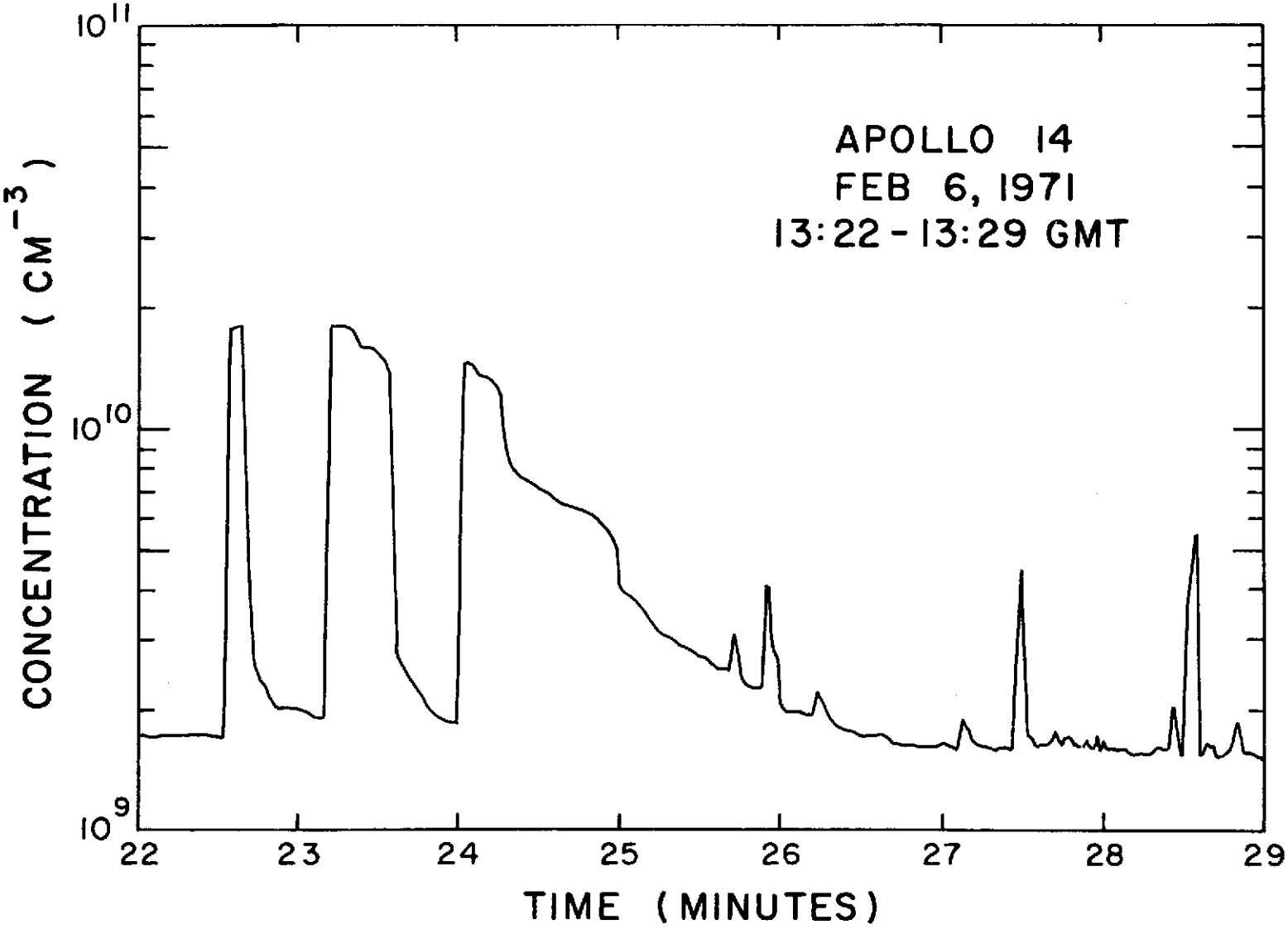

Figure 29 Concentration at Apollo 14 site at time of final depressurization of Lunar Module and jettison of unneeded hardware.

were more than a few hundred meters away, as the variation in molecular velocities would spread out the sharp rise with the faster moving particles arriving before the slower.

Data Availability Through NSSDC

The data listed in Tables 5 and 6 are available at NSSDC on 35 mm film in the form shown in Figures 14 - 17.

The method chosen for presentation of the data is a microfilm plot with concentration shown in the bottom half of the frame and the gauge temperature in the top half. The times used on all of the frames are GMT, following the day of the year. In the normal operating mode of the instrument, an average of four data points are obtained each minute. The data are recorded with approximately 15 hours of data on each frame. The concentration is plotted logarithmically on a scale from 10^5 to 10^{11} particles/cm^3, and the temperature is plotted linearly on a scale from 0 K to 400 K. The values shown on the plots have been computed using the calibration curves of the appropriate gauge and temperature sensor.

Acknowledgment

We specially acknowledge the cooperation and assistance of Mr. Frank Torney at Norton Research Corporation in connection with the gauge, Dr. John Freeman at Rice University in connection with the

gauge electronics, Dr. George Chang at Bellcomm, Inc. in connection with the lunar environment. Mr. James Sanders at NASA Johnson Space Center and Mr. Derek Perkins at Bendix Aerospace Systems Division in connection with the incorporation of the gauge into the ALSEP, Mr. Charles Gosselin at Midwest Research Institute in connection with the gauge calibration, and many others too numerous to mention throughout the Apollo project.

REFERENCES

Bame, S. J., J. R. Asbridge, A. J. Hundhausen, and M. D. Montgomery (1970), Solar wind ions: $^{56}Fe^{+8}$ to $^{56}FE^{+12}$, $^{28}Si^{+7}$, $^{28}Si^{+8}$, $^{28}Si^{+9}$, and $^{16}O^{+6}$, J. Geophys. Res., 75, 6360-6325.

Buehler, F., H. Gerutti, P. Eberhardt, and J. Geiss (1972), Results of the Apollo 14 and 15 solar wind composition experiment (abstract), "Revised Abstracts of the Third Lunar Science Conference," p. 102, January.

Cameron, A. G. W. (1971), A new table of abundances in the solar system, in Origin and Distribution of the Elements, edited by L. H. Ahrens, Pergamon, New York, 124-145.

Eberhardt, P., J. Geiss, H. Graf, N. Grogler, U. Krahlenbuhl, H. Schwaller, J. Schwarzmuller, and A. Stettler (1970), Trapped solar wind noble gases, exposure age, and K/Ar age in Apollo 11 lunar fine material, Proc. Apollo 11 Lunar Sci. Conf., Geochim. Cosmochim. Acta Suppl. 1, Vol. 2, pp. 1037-1070, Pergamon Press.

Geiss, J., F. Buehler, H. Gerutti, P. Eberhardt, and J. Meister, (1971) The solar wind composition experiment, Apollo 14 Preliminary Science Report, NASA SP 272, pp. 221-226.

Hundhausen, A. J. (1970) Composition and dynamics of the solar wind plasma, Rev. Geophys. Space Phys., 8, 729-811.

Hundhausen, A. J., S. J. Bame, J. R. Ashridge and S. J. Sydoriak (1970) Solar wind proten properties: Vela 3 observations from July 1965 to June 1967, J. Geophys. Res., 75, 4643-4657.

Hodges, R. R., Jr., J. H. Hoffman and F. S. Johnson, (1973) Lunar atmosphere, to be published in ICARUS.

Hodges, R. R., Jr. and F. S. Johnson (1968), Lateral transport in planetary exospheres, J. Geophys. Res., 73, 7307-7317.

Johnson, F. S. (1971), Lunar atmosphere, Rev. Geophys. Space Phys., 9, 913-923.

Jokipii, J. R. (1971), Propagation of cosmic rays in the solar wind, Rev. Geophys. Space Phys., 9, 27-87.

Manka, R. H. and F. C. Michel (1971), Lunar atmosphere as a source of lunar surface elements, Proc. Second Lunar Science Conference, Vol. 2, MIT Press, 1717-1728.

Manka, R. H., F. S. Michel, and J. W. Freeman (1972), Evidence for acceleration of lunar ions (abstract) "Revised Abstracts of the Third Lunar Science Conference," p. 504, January.

Ness, N. F., K. W. Behannon, C. S. Scearce, and S. C. Cantarano (1967), Early results from the magnetic field experiment on lunar Explorer 35, J. Geophys. Res., 72, 5769-5778.

Owens, C. L., Ionization gauge calibration system using a porous plug and orifice, J. Vac. Sci. Technology, 2, 104, (1965).

Smith, Alphonsa, Analysis of a molecular beam system utilizing a down pressure source, NASA TN D-5308, July 1969.

Sonett, C. P., and D. S. Colburn (1967), Establishment of a lunar unipolar generator and associated shock and wake by the solar wind, Nature, 216, 340-343.